DEVELOPMENT OF VANADIUM-PHOSPHATE CATALYSTS FOR METHANOL PRODUCTION BY SELECTIVE OXIDATION OF METHANE

FINAL REPORT

Robert L. McCormick (Principal Investigator)

October 1, 1997

DOE Contract No. DE-AC22-92PC92110

Department of Chemical Engineering and Petroleum Refining
and
Colorado Institute for Fuels and High-Altitude Engine Research

Colorado School of Mines
Golden, Colorado 80403-1887

DRAFT

DISCLAIMER

TABLE OF CONTENTS

LIST OF FIGURES

LIST OF TABLES

EXECUTIVE SUMMARY

This DOE sponsored study (DE-AC22-92PC92110) of methane partial oxidation was initiated at Amax Research and Development in Golden, Colorado in October of 1993. Shortly thereafter the management of Amax closed this R&D facility and the PI moved to the Colorado School of Mines. The project was begun again after contract transfer via a novation agreement. Experimental work began with testing of vanadyl pyrophosphate (VPO), a well-known alkane selective oxidation catalyst. It was found that VPO was not a selective catalyst for methane conversion yielding primarily CO. However, promotion of VPO with Fe, Cr, and other first row transition metals led to measurable yields for formaldehyde, as noted in the summary table. Catalyst characterization studies indicated that the role of promoters was to stabilize some of the vanadium in the V^{5+} oxidation state rather than the V^{4+} state formally expected for $(VO)_2P_2O_7$.

Yields with vanadium phosphate catalysts were extremely low and it was decided to pursue another strategy. A catalytic material with the metal in a higher rather than a lower oxidation state (r.e. V^{5+} versus V^{4+}) was preferred. Given that Fe successfully promoted VPO, and given Wang and Otsuka's (1995) report that $FePO_4$ had interesting properties for methane oxidation, this phosphate was selected for additional study. Note that in $FePO_4$ iron is in the 3+ oxidation state and so can be reduced to Fe^{2+}. $FePO_4$ (quartz polymorph) is a much more active and selective catalyst than VPO, producing formaldehyde at nearly two orders of magnitude higher yield (see summary table). When this material was supported on silica, yield again nearly doubled. Inclusion of steam in the feed gas lead to a further doubling of yield. Measurable but low yields of methanol were also observed.

Kinetic Parameters and Yields for CH_4 Oxidation over Various Catalysts.

Catalyst	Reaction Order			Activation Energy, kJ/mol	Maximum Space Time Yield, g/kg-h	
	CH_4	O_2	H_2O		HCHO	CH_3OH
$(VO)_2P_2O_7$	0.73	0.08	--	102	0	0
$(VO)_2P_2O_7$-Fe	--	--	--	96	1.5	0
$(VO)_2P_2O_7$-Cr			--	95	2.0	0
$FePO_4$ (Q)	0.66	0.45	--	81	59 148[a]	0
SiO_2 OR	0.93	0.31	--	142	96	0
$FePO_4/SiO_2$	0.61	0.28	--	129	240	5
	0.48	0.21	0.23	--	487	8

[a]In the presence of steam.

Water was observed to enhance selectivity over silica supported iron phosphate and to enhance the reaction rate as well. The fact that water enhances selective product yields and exhibits a positive effect on the methane conversion rate strongly suggests the formation of a new active site under our reaction conditions, possibly a hydroxyphosphate phase. Another extremely interesting feature of the silica supported iron phosphate catalyst is that high formaldehyde yields could be obtained at very low methane to oxygen ratios (even below 1). This behavior is unusual in methane partial oxidation and may have significant practical and economic implications, notably elimination of the need to use pure oxygen.

Aspects of the work described in this final report have been presented at the 1997 North American Catalysis Society Meeting in Chicago and will appear shortly in a refereed journal. A second journal article is currently undergoing peer review and a third is in preparation. Results for the iron phosphate materials will be presented at the 1997 AIChE Meeting in Las Angeles. Additional articles may ultimately be prepared.

1. INTRODUCTION

This report describes results obtained under Contract No. DE-AC22-92PC92110 "Development of Vanadium-Phosphate Catalysts for Methanol Production by Selective Oxidation of Methane". This project was initiated on October 1, 1992 at Amax Research and Development, Inc. in Golden, Colorado. Amax R&D was closed at the end of 1993 in a corporate merger. The principal investigator, Robert L. McCormick, joined the faculty of the Colorado School of Mines and the project was continued after contract transfer via a novation agreement which took effect on July 1, 1994.

The United States has vast natural gas reserves that could contribute significantly to our energy security if economical technologies for conversion to liquid fuels and chemicals were developed. Many of these reserves are small scale or in remote locations and of little value unless they can be transported to consumers. For natural gas, transportation is economically performed via pipeline, but this route is usually unavailable in remote locations. Another option is to convert the methane in the gas to liquid hydrocarbons such as methanol, which can be transported easily and economically by truck. Therefore, the conversion of methane to liquid hydrocarbons has the potential to decrease our dependence upon oil imports by opening new markets for natural gas and increasing its use in the transportation and chemical sectors of the economy.

The goal of this project is to develop a catalyst that allows methane oxidation to methanol to be conducted at high conversion and selectivity. To achieve a high conversion, we require a catalyst that is active at less than 500ºC to enhance selectivity and allow higher feed gas oxygen content. Ideally, air would be used as the source of oxygen although this does not appear to be a viable approach now. Achievement of high selectivity will require a highly selective catalyst and optimization of process conditions. Vanadyl pyrophosphate was selected for study because of demonstrated high selectivity in oxidation of other alkanes at relatively low temperature, and is used commercially.

The primary commercial use of vanadium phosphate (VPO) catalysts is in C_4 hydrocarbon oxidation to maleic anhydride. These catalysts have also shown good activity for conversion of ethane (Michalakos et al., 1993), propane (Ai, 1986), and pentane (Busca and Centi, 1989), as well as butane (Centi, et al., 1988). Methane oxidation is a much more difficult reaction to catalyze than that of other alkanes, and it is expected that considerable modification of vanadyl pyrophosphate will be required for this application. It is well known that VPO can be modified extensively with a large number of different promoters and in particular that promoters can enhance selectivity and lower the temperature required for butane conversion (Hutchings, 1991).

The catalytically active phase in VPO catalysts is vanadyl pyrophosphate, $(VO)_2P_2O_7$ (Cavani and Trifiro, 1994). The catalyst is prepared from V_2O_5 and phosphoric acid. The most active and selective catalysts are obtained using organic solvents such as a mixture of isobutyl and benzyl alcohols and anhydrous phosphoric acid (Cavani and Trifiro, 1994; Cornaglia, et al., 1993a; Busca, et al., 1986a). Excess phosphorus is generally employed in the reaction mixture (Centi, et al., 1988; Horowitz, et al., 1988; Hodnet, 1985). The catalyst precursor obtained from reaction of these materials under reflux is $VO(HPO_4)\cdot 0.5H_2O$ which has a layered structure. The

use of organic solvents and excess phosphorus is thought to lead to a desirable crystalline face exposure. The preparation also leads to development of disorder in the stacking plane through entrapment of benzyl alcohol molecules between the layers (Horowitz, et al., 1988; Busca, et al., 1986a). This procedure may also introduce anion vacancies (Cornaglia, et al., 1991).

The catalyst precursor is then converted to vanadyl pyrophosphate by heating under a variety of gas environments. The precursor undergoes a topotactic transformation (Johnson, et al., 1984) such that structural disorder in the precursor stacking plane is preserved in the active phase (Busca, et al., 1986a). This structural disorder has been proposed to lead to the formation of very strong Lewis acid sites (Busca, et al., 1986b) which are may be the source of the catalysts ability to activate alkanes. However, equilibrated catalysts (used for at least 200 hours) exhibit a lower degree of structural disorder but a higher level of strong Lewis acidity as compared to freshly activated catalysts (Cornaglia, et al., 1993b). Thus, the source of the strong Lewis acidity is not well understood. One hypothesis is that anion vacancies are introduced by organic solvents and excess phosphorus. These vacancies are the source of both disorder in the stacking plane and the strong Lewis acidity. After many hours on stream, the structural disorder is eliminated but the anion vacancies remain (Cornaglia, et al., 1991). After the activation process some carbon is present on or in the catalyst which may also contribute to structural disorder or to the active site structure (Busca and Centi, 1989; Pepera, et al., 1985). The P:V ratio of the active catalyst is typically about 1.05, assuming some excess phosphorus was present, regardless of the starting P:V ratio (Horowitz, et al., 1988). Most or all of the excess phosphorus is found on the surface. Here the P:V ratio has been found to be closer to 2. This observation has lead to a model of the VPO surface consisting of pendant pyrophosphate groups (Ebner and Thompson, 1993).

Prior to the present work, the catalytic activity of $(VO)_2P_2O_7$ for oxidation of methane had not been reported. Here we report the results of methane oxidation measurements on this catalysts as well as results for oxidation of methanol, formaldehyde, and dimethyl ether (DME). The catalyst is not selective for methane oxidation producing primarily CO, so several methods of modifying the catalyst to improve selectivity were attempted. One study examined the impact of modifying surface acidity, which was found to have little effect. A second study examined several first row transition metals as promoters. Fe and Cr were found to lead to small improvements in selectivity for production of formaldehyde. These experiments led us to examine iron phosphates as methane oxidation catalysts. It was found that $FePO_4$, and especially $FePO_4$ supported on silica, exhibit reasonably high activity for conversion of methane to formaldehyde, low but measurable activity for formation of methanol.

2. PROJECT DESCRIPTION

2.1. Objectives

The objectives of this project are:

- To determine optimum conditions for methanol and formaldehyde production from methane using VPO catalysts.
- To utilize promoters and catalyst supports to improve oxygenate yield relative to the base case catalysts.

- To provide a preliminary understanding of how these promoters and supports actually effect catalyst properties.
- Use the information obtained to prepare advanced catalysts that will be tested for activity, selectivity, and stability.

2.2. Project Overview

The goal of the project was to develop a catalyst that allows methane oxidation to methanol to be conducted at high conversion and selectivity. The catalyst development strategy is to utilize promoters and supports to improve the activity and selectivity of the unmodified VPO catalyst.

The project was divided into four tasks:

Task 1: Laboratory Setup.
Task 2: Process and Catalyst Variable Study.
Task 3: The Effect of Promoters and Supports.
Task 4: Advanced Catalyst Testing.

Laboratory setup, Task 1, was performed two times at both Amax R&D and at Colorado School of Mines. Work on each of the other tasks has been completed and a brief overview, in terms of catalyst systems studied rather than tasks, is given below.

2.2.1. Oxidation by $(VO)_2P_2O_7$. Partial oxidation of methane by molecular oxygen over vanadyl pyrophosphate has been studied in the temperature range of 573-698 K and atmospheric pressure. Carbon monoxide, carbon dioxide and water were found to be the principal reaction products. Macrokinetic parameters for the methane oxidation reaction were determined. A simple power law rate expression fit the rate data well over the whole temperature range. The rate of reaction of methane was 0.08±0.02 order in oxygen partial pressure, 0.73±0.07 order in methane partial pressure, and the activation energy was found to be 102±6 kJ/mole. The catalytic oxidation of methanol, dimethyl ether, and formaldehyde over vanadyl pyrophosphate has been examined under both differential and integral reactor conditions. Temperatures of 400-650 K and GHSV of 3,000-15,00 hr^{-1} were employed over a range of hydrocarbon and oxygen partial pressures. Reaction networks are proposed where methanol is converted via parallel reactions to dimethyl ether and formaldehyde. Dimethyl ether is converted in parallel reactions to methanol and carbon dioxide. Formaldehyde oxidation is facile over this catalyst producing CO and CO_2 in sequential reactions. Global reaction orders were determined from differential reactor data and suggest that overall, these reactions are first order in hydrocarbon and zero order in oxygen.

2.2.2. Modification of Surface Acidity. It has been shown that strong Lewis acid sites on the surface of VPO are responsible for initial alkane activation (Busca, et al., 1986a). This Lewis acidity is thought to be caused by lattice defects or strain initiated by disorder in stacking of the layers of VPO (Busca, et al, 1986b; Horowitz, et al, 1988). We attempted to increase the strength of these strong Lewis acid sites by enhanced strain or disorder in the layer stacking. By increasing Lewis acid site strength it is hoped that the temperature required for methane

activation can be lowered resulting in improved selectivity. The degree of disorder of these materials was measured by XRD line broadening. Surface acidity of these materials was measured by FTIR of chemisorbed bases and by activity in methanol coupling to dimethyl ether. Activity and selectivity in methane oxidation were also measured. XRD indicates that modifications were successful at introducing disorder in the layer stacking. The methanol conversion results suggest that these catalysts do have more acid sites. IR suggests that sites on one of the catalysts may be of higher strength but the results are not conclusive. The catalysts with enhanced acidity as gauged by methanol conversion were not more active or selective for methane conversion.

2.2.3. Promotion by First Row Transition Metals. Vanadyl pyrophosphate samples promoted with Mn, Cr, Fe, Co, Cu, and Zn have been prepared by addition of promoter salts to a suspension of the activated catalyst. In preliminary screening experiments promotion with Fe and Cr produced significant changes in selectivity with measurable yields of formaldehyde at low conversions. Partial oxidation of methane by molecular oxygen over Cr and Fe promoted vanadyl pyrophosphate catalysts has been studied in detail in the temperature range of 573-698 K and atmospheric pressure. High formaldehyde selectivity was observed at very low methane conversion levels with HCHO space time yields in the range of 0.5 to 2.0 g/kg-h. As the extent of the reaction was increased selectivity to formaldehyde decreased rapidly, and changes in selectivities with conversion indicate a sequential conversion of methane to formaldehyde, CO, then CO_2. The activation energy was found to be 102±6 kJ/mole, unchanged by promotion with Fe and Cr. Analysis by XPS and ICP-AA indicates that promoters were incorporated equally into the bulk and surface of these catalysts. XPS indicates an increase in the average surface oxidation state of vanadium in the promoted catalysts and XRD shows that promotion causes oxidation of a small fraction of the pyrophosphate to form α_{II}-$VOPO_4$. ^{31}P NMR spin-echo mapping confirms the enhanced formation of V^{5+} in the promoted samples. The presence of V^{5+} may therefore be required for the formation of selective products. It is proposed that the role of promoters is to increase the rate of formation of V^{5+} during activation, or stabilize V^{5+} containing domains under the highly reducing methane oxidation conditions.

2.2.4. Oxidation by $FePO_4$ Based Catalysts. Crystalline $FePO_4$ was tested in methane oxidation because of the interesting results noted for Fe promotion of vanadium phosphate and because of literature reports suggesting that it was an active and selective catalyst. $FePO_4$ and $FePO_4$ supported on silica produce much higher yields of partial oxidation products from methane than VPO. The most selective catalyst examined to date is $FePO_4$ supported on silica. This material has produced formaldehyde with space time yields of nearly 500 g/kg-h, if steam is included in the feed gas. Methanol yields are low but quantifiable at roughly 10 g/kg-h. Addition of water to the feed gas produces large improvements in the formaldehyde yield by suppression of the parallel reaction to form carbon dioxide. Increasing oxygen partial pressure over this catalyst did not produce the expected drop in formaldehyde yield and in fact, formaldehyde yield actually increased.

3. EXPERIMENTAL METHODS

This chapter describes methods of catalyst testing and characterization employed in the project. A number of different catalyst synthesis procedures were employed and these are described separately with the results.

3.1. Methane Oxidation Reactor

Steady-state reaction studies were performed in a fixed-bed micro-reactor. The composition (CH_4, O_2, He) and flow rate of the feed gas was controlled by Brooks 5850E mass flow controllers. Methanol was introduced to the system by passing the O_2/He mixture through a series of sealed flasks maintained at 20^{o}C. Here the desired methanol concentrations were achieved by controlling the temperature of the saturator and the flow rate of the stream through the flasks. Formaldehyde introduction was performed in a similar way by placing paraformaldehyde in the saturator and heating with a thermostated oil bath. The concentration of formaldehyde was varied by adjusting the saturator temperature between 40-65°C. Figure 3-1 shows vapor phase formaldehyde concentration as a function of saturator temperature. In a typical run, saturator temperature was maintained at 50°C to obtain about 10% formaldehyde in the feed stream. DME was fed to the system through the recalibrated helium mass flow controller as a 5.31% DME-helium mixture.

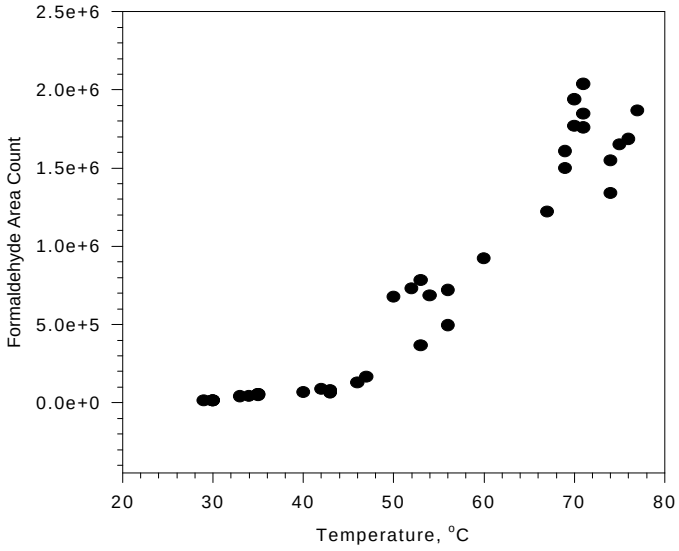

Figure 3-1. Vapor phase formaldehyde concentration (as GC area count) versus paraformaldehyde decomposition/vaporization temperature.

The reactor was a quartz tube, 30 cm long and 1.0 cm i.d. at the catalyst bed portion, mounted vertically in a tubular furnace. A quartz frit was used to hold the catalyst bed in place. Typically about 0.3 g of catalyst (screened to 0.5-0.7 mm particle size, 0.677 g/cm^3 bulk density) was loaded into the reactor and covered with 15 mm layer of quartz beads to obtain a preheating zone and a uniform gas distribution. The exit diameter was decreased to 5 mm i.d. right after the quartz frit to allow reaction products to leave the heated zone more rapidly. Temperature was monitored by two K-type thermocouples, one placed in contact with the catalyst bed, the other right under the frit. Prior to reaction the catalyst was calcined in situ under helium flow (20

ml/min) at the reaction temperature for 1 hour. Methane was introduced into the reactor first so that at all times the methane-oxygen mixture was kept well above the upper explosive limits. Methane conversion was well below 10% for all experiments reported. Overall carbon balance closures obtained were within ± 5% and mostly within ± 3%. Fractional conversion and selectivity were defined as:

$$Conversion = \frac{moles \quad (HCHO + CO + CO_2) \quad formed}{moles \quad CH_4 \quad fed}$$

$$Selectivity = \frac{moles \quad product \quad formed}{moles \quad (HCHO + CO + CO_2) \quad formed}$$

3.2. Product Analysis

An on-line Hewlett-Packard 5890 Gas Chromatograph (GC) equipped with a thermal conductivity detector was used to analyze reactant and product streams. Separation of CH_4, O_2, CO, and CO_2 was accomplished with a 6'x 1/8'' S.S. Carbosphere 80/100 column. For methanol, formaldehyde, DME and water an 8'x 1/8'' S.S. Poropak-T column was used. For the Carbosphere column a GC temperature program starting at 323 K and ending at 403 K was applied, with an initial soak time of 3 minutes and a heating rate of 30 K/min. For the Poropak-T column, the GC temperature was held constant at 403 K. Calibration for CH_4, DME, CO, and CO_2 was accomplished using standards from Scott Specialty Gases. Methanol and water calibrations were performed using standard solutions of reagent grade methanol and deionized water prepared in volumetric flasks. These were injected with a 0.5 μL syringe to obtain calibration curves that are shown in Figures 3-2 and 3-3.

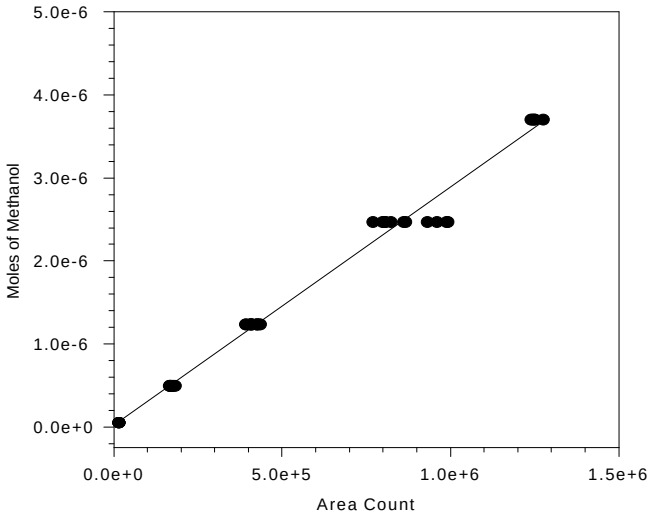

Figure 3-2. GC calibration for methanol.

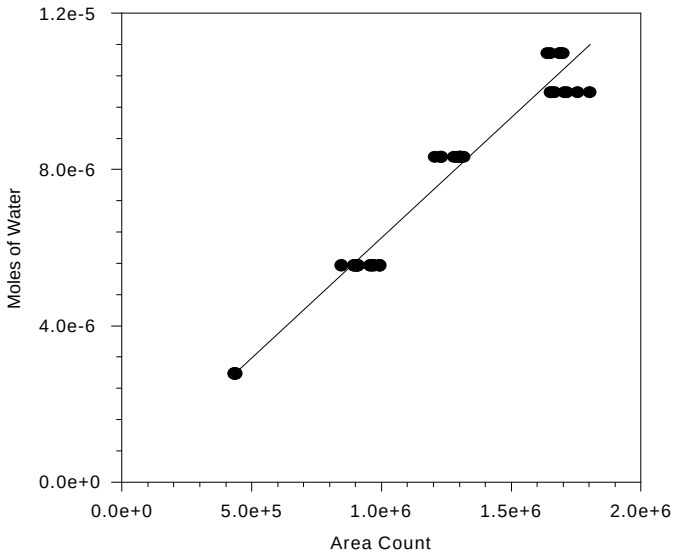

Figure 3-3. GC calibration for water.

Calibration of the GC for formaldehyde is more complex. Paraformaldehyde was placed in a heated flask, purged by the feed gas. A feed gas of oxygen-helium was passed through the system and analyzed to obtain a formaldehyde peak area. The mixture was then passed over a 4 wt% Pd/Al_2O_3 combustion catalyst at 673 K. Complete formaldehyde conversion was obtained and CO_2 was the only combustion product. The known CO_2 calibration was then used to determine the concentration of formaldehyde in the feed gas. This concentration and the formaldehyde peak area constitute a calibration curve for formaldehyde which is shown in Figure 3-4. This calibration was cross-checked with Romjin's iodometric titration as follows. The feed stream, 10% formaldehyde in concentration, was bubbled through water in a sealed 200 ml glass container which was immersed in an ice-water bath to absorb any condensable material. The solution obtained was then mixed with a known excess of iodine in 5M NaOH to yield formic acid and iodide. Unreacted iodine was titrated with thiosulfate in presence of starch as indicator. The difference between the initial amount of iodine and that of measured in the titration was used to quantify the formaldehyde in the feed stream.

3.3. Catalyst Characterization

3.3.1. Surface Area Measurement. Specific surface areas (BET) of the catalyst samples were measured using a Micromeretics 2100E Accusorb Instrument. Nitrogen was used as adsorbate at liquid nitrogen temperatures, taking a value of 0.162 nm^2 for the cross section area of the adsorbed nitrogen molecule.

3.3.2. Chemical Analysis. Chemical analysis was performed by ICP-AA on samples digested in concentrated nitric acid and then diluted before analysis.

3.3.3. X-ray Powder Diffraction. X-ray powder diffraction (XRD) patterns were obtained using a Rigaku diffractometer. Cu K_α radiation (λ=1.5432 Å) was used as the incident X-ray source.

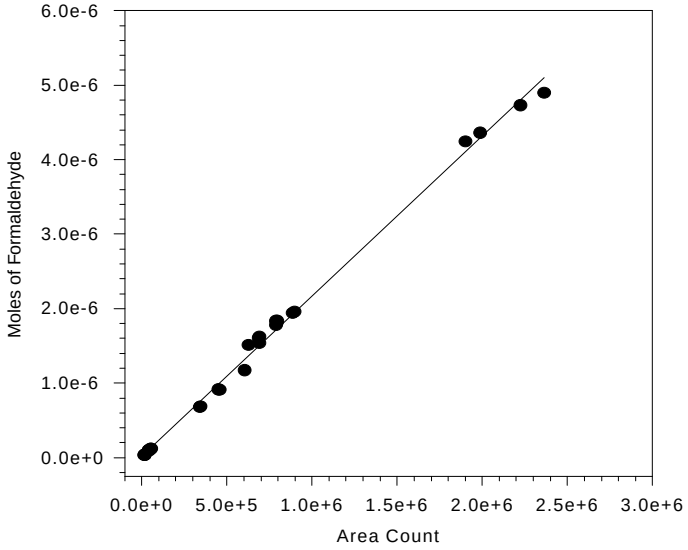

Figure 3-4. GC calibration for formaldehyde.

3.3.4. ^{31}P NMR Spectroscopy. Wide line (non-spinning) ^{31}P NMR experiments were conducted on a Chemagnetics CMX Infinity 400 instrument (7.5 mm probe, ^{31}P spectral frequency of 162.0 MHz) using a spin-echo mapping approach similar to that described by Li and coworkers (1991). In our implementation of this method the carrier frequency was varied in increments of 62.5 kHz above and below the resonance frequency of ^{31}P in 85% H_3PO_4 to cover the complete range where spectral intensity was observed.

3.3.5. X-ray Photoelectron Spectroscopy. A Kratos Electronics spectrometer with monochromatic Al K_α radiation was used to obtain the X-ray photoelectron spectra (XPS). The binding energy of C 1s (284.6 eV) was used as a reference in these measurements. Deconvolution of the V $2p_{3/2}$ binding energy envelope was performed by fitting two Gaussian peaks separated by 1 to 1.1 eV with a non-linear regression package varying intensity and peak width.

3.3.6. Infrared Spectroscopy. Infrared spectra were obtained by diffuse reflectance on a BioRad FTS-40 instrument using a Harrick diffuse reflectance attachment and samples mixed with KBr. Infrared spectra of adsorbed bases were recorded on the Bio-Rad FTS-40 spectrometer in the FT mode using an MCT detector with 2 cm^{-1} resolution. Samples were held in the heatable cell of a Harrick diffuse reflectance attachment enclosed in a dome containing KBr windows. The sample was conditioned in a flow of He by heating to 673 K, holding the temperature for 30 minutes, and then cooling to 300 K and holding that temperature for 30 minutes. The He flow was then saturated with anhydrous base for 10 minutes then purged with He for a further 10 minutes. The sample was then heated to the desired temperature for recording of spectra. Infrared spectra of KBr pellets were acquired on the same instrument.

3.3.7. Mossbauer Spectroscopy. The samples were diluted in powdered sugar to avoid a too high Mössbauer absorption, and pressed into pellets. The spectra were recorded at room

temperature, using a 25 mCi ^{57}Co/Rh source and a conventional constant acceleration spectrometer, operated in triangular mode. Data acquisition was done with standard multichannel scaling and data analysis were performed by least square fit of superposition of Lorentzian lines (some symmetry restrictions applied). By computer folding and fitting, isomer shifts (δ) with respect to α-Fe, quadrupole splitting (Δ) and the line widths (W) were calculated with a precision about 0.01 mm.s^{-1}. The accuracy for hyperfine fields (H) determinations was 0.2 kOe.

4. PRELIMINARY RESULTS

This chapter describes preliminary experiments performed to verify our experimental setup and insure that high quality data would be obtained.

4.1. Blank Reactor Runs

Results of blank methane and methanol oxidation tests are shown in Table 4-1. At atmospheric pressure no methane conversion was observed at temperatures as high as 873 K. A somewhat surprising result is the lack of significant methanol conversion at atmospheric pressure and temperatures up to 823 K. In vanadium phosphate catalyst development we are endeavoring to convert methane at temperatures of 773 K and below. These blank reactor results suggest that gas phase reactions are not important at atmospheric pressure in this temperature range. Oxidation of methane and methanol did occur at higher pressures. Non-catalytic methanol oxidation produced primarily carbon oxides although formaldehyde and methane were also observed.

Table 4-1. Results of Non-Catalytic Oxidation of Methane and Methanol in Quartz Lined Reactor (GHSV=8000@NTP).

Temperature,	Feed Composition (balance He)			Pressure,	Percent	Percent Selectivity				
°C	%O_2	%CH_4	%CH_3OH	atm	Conversion	CO	CO_2	HCHO	CH_3OH	CH_4
400	10	20	0	6.8	0	0	0	0	0	--
450	10	20	0	6.8	0	0	0	0	0	--
450	10	20	0	15.3	0	0	0	0	0	--
500	10	20	0	5.1	0.06	0	100	0	0	--
500	10	20	0	6.8	0.11	78.1	21.8	0	0	--
500	10	20	0	10.2	0.81	5.3	16.6	0	78.0	--
500	10	20	0	15.3	31.1	63.4	23.3	0.89	12.3	--
525	10	20	0	6.8	45.8	55.6	18.2	0	26.2	--
525	10	20	0	10.2	56.4	65.3	16.1	0.25	18.3	--
550	10	20	0	1	0	0	0	0	0	--
550	10	20	0	5.1	1.3	21.2	37.8	0	40.9	--
550	10	20	0	6.8	49.5	61.7	24.3	0	13.9	--
600	10	20	0	1	0	0	0	0	0	--
525	10	0	20	1	0.2	14.1	53.9	31.9	0	0
525	10	0	20	5.1	96.5	49.0	50.3	0	0	0.7
550	10	0	20	1	0.2	22.2	12.8	0	0	64.8
550	10	0	20	5.1	80.3	84.2	10.4	0.86	0	4.4

4.2. Tests for Mass Transfer Limitations

Tests for internal transport limitations were conducted by varying catalyst particle size while maintaining constant GHSV and feed gas composition. The experiments conducted using a ZnO promoted vanadyl pyrophosphate are listed in Table 4-2. The only reaction product observed was CO and carbon balances were always in excess of 97%. The results for two temperatures are shown in Figure 4-1. Conversions are low under these conditions however they appear to be constant for all but the largest particle diameter. We do not believe that pore diffusion limitations are becoming important for this particle size but rather that the reactor diameter/particle diameter ratio has become so small that gas-solid contacting is poor. The quartz reactor diameter was 14 mm in these experiments.

Table 4-2. Experiments conducted to test for internal transport limitations. (CH_4:O_2=10, 450 and 748 K).

Mean Diameter, mm	**1.696**	**1.122**	**0.711**	**0.504**	**0.315**	**0.181**
Mesh Range	10-14	14-20	20-28	28-40	40-70	70-100
Weight, g	0.506	0.501	0.503	0.507	0.500	0.502
Volume, cc	0.90	0.85	0.85	0.82	0.80	0.80
Flowrate, ml.min	33.0	30.8	30.8	29.7	29.1	29.1
GHSV, hr^{-1}	2200	2174	2174	2173	2183	2183

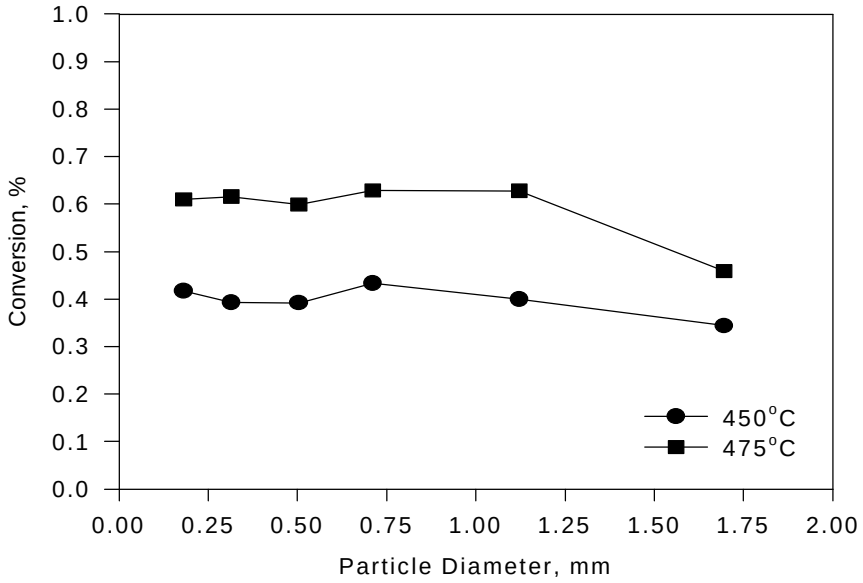

Figure 4-1. Conversion versus particle diameter data, testing for pore diffusion limitations.

Tests for external transport limitations were conducted at GHSV of 2300 hr^{-1} with flow rates of 62 and 31 ml/min and bed volumes of 1.6 and 0.82 ml, respectively. The ZnO promoted VPO catalyst was employed with a CH_4:O_2 ratio of 10. Temperature was varied from 673 to 748 K. For conditions where external transport is significant lower gas flowrate should yield a lower conversion even though GHSV is the same. Results are shown in Figure 4-2. For temperatures

of 723 K and greater transport limitations are evident in that higher conversion is observed at higher flow rate. Thus, considerably higher flow rates are required if temperatures are to exceed this value. In the testing performed under this contract additional experiments of this type were always performed to insure the absence of external transport limitations.

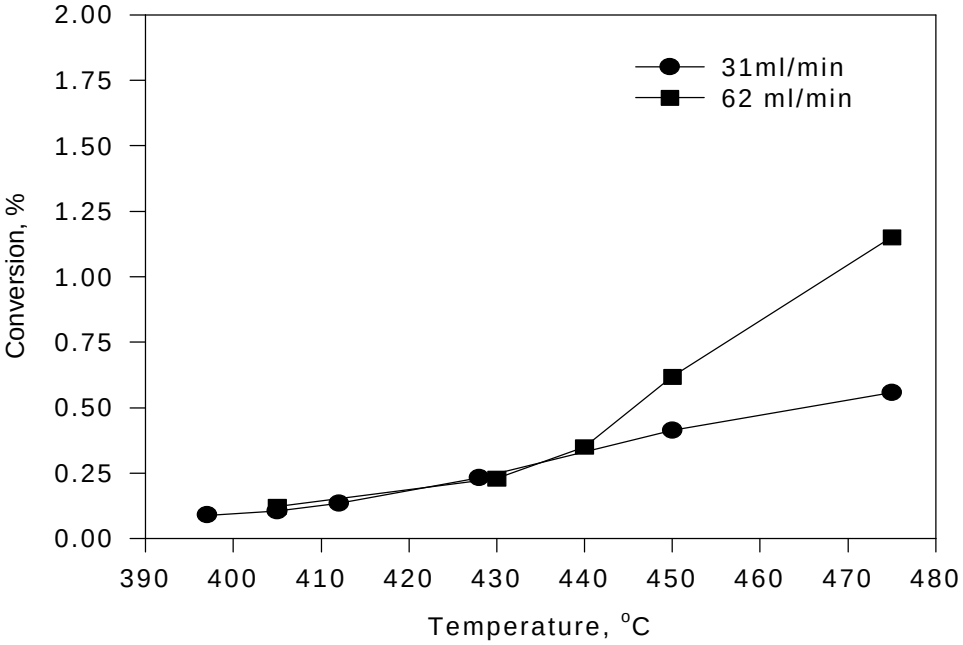

Figure 4-2. Conversion versus temperature at two flow rates and constant GHSV, testing for external transport limitations.

5. RESULTS

5.1. Oxidation by $(VO)_2P_2O_7$

5.1.1. Catalyst Synthesis. Vanadyl pyrophosphate was prepared following the procedure reported by Busca and coworkers (1986a). Fifteen grams of V_2O_5 was suspended in 90 ml of isobutyl alcohol and 60 ml of benzyl alcohol. The suspension was stirred under reflux for 3 hours, then cooled to room temperature and left stirring overnight. Then 16.2 g 99% anhydrous phosphoric acid was added (P:V atomic ratio 1.00), and the mixture was refluxed for an additional 2 hours. After completion of the reaction, the solid phase was recovered by filtration, washed with isobutyl alcohol and dried in air at 393 K overnight. The dried catalyst precursor, $VOHPO_4$-$0.5H_2O$, was then calcined in a 1.5% butane in air at 673 K for 18 hours (GHSV 800 h^{-1}) to facilitate the transformation to vanadyl pyrophosphate.

5.1.2. Catalyst Characterization. X-ray diffraction data obtained for the precursor show the peaks of vanadyl phosphate hemihydrate $VOHPO_4$-$0.5H_2O$. A poorly crystalline vanadyl pyrophosphate was the only phase observed by XRD in the activated sample in agreement with the results reported for this preparation method. Given the broadness of some of the XRD peaks the presence of other VPO phases cannot be completely ruled out, however. After exposure to methane oxidation conditions for 20 hours the (200) reflection at 22.8° has increased in intensity, suggesting that order in the layer stacking direction has increased. ICP-AA indicated a bulk P:V

ratio of 0.97 and XPS indicated a surface P:V ratio of 1.23. The BET surface area was 32.1 m^2/g, bulk density was 0.752 g/cm^3, and particle size was 28-40 mesh.

5.1.3. Reaction Studies: Methane. The principal products of methane oxidation over VPO were found to be carbon monoxide and carbon dioxide. Formaldehyde was found only in trace quantities. Figure 5-1 presents selectivities to these products as a function of conversion, varied by varying temperature and GHSV for two different methane to oxygen ratios. As shown, carbon monoxide is the primary product and CO selectivity decreases as the conversion increases. At zero conversion, CO selectivity approaches 100% suggesting that methane is oxidized directly to carbon monoxide and that any methoxy or formate surface intermediate is very rapidly converted under these conditions. Carbon dioxide was never a significant product at very low methane conversion levels, which is an indication of no direct oxidation route from methane to carbon dioxide. CO selectivity is higher at the higher methane to oxygen ratio, as expected because less oxygen is available.

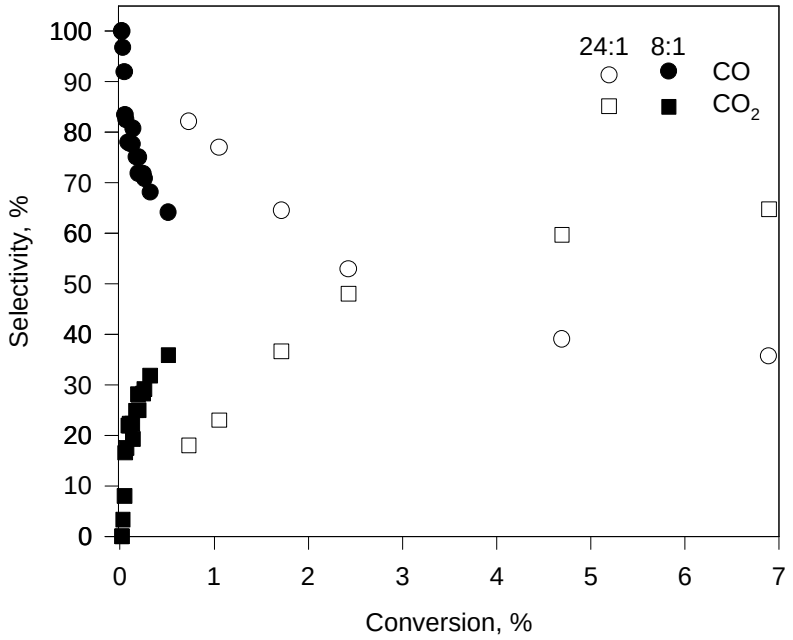

Figure 5-1. Product selectivity as a function of methane conversion for vanadyl pyrophosphate. GHSV=1400-13,500 h^{-1}, P_{CH4}=97 kPa P_{O2}=4 kPa (24:1) P_{CH4}=43 kPa, P_{O2}=5 kPa (8:1), T=573-698 K.

To determine the reaction orders, methane partial pressure was changed from 21 to 65 kPa, keeping the oxygen partial pressure constant at 8 kPa. During these runs, gas hourly space velocity (GHSV) was also kept constant at 2700 h^{-1}. In a similar set of experiments at the same GHSV oxygen partial pressure was changed from 8 to 32 kPa, keeping methane pressure constant at 42 kPa. The effect of reactant partial pressures on the observed rate is shown in Figure 5-2. The data indicate that the reaction order for methane was 0.73±0.07 (indicated confidence intervals are standard error). The rate of reaction of methane showed a very small positive order in oxygen of about 0.08±0.02, provided that oxygen conversion was kept below 100%. Both reaction orders were not affected by temperature over the range studied.

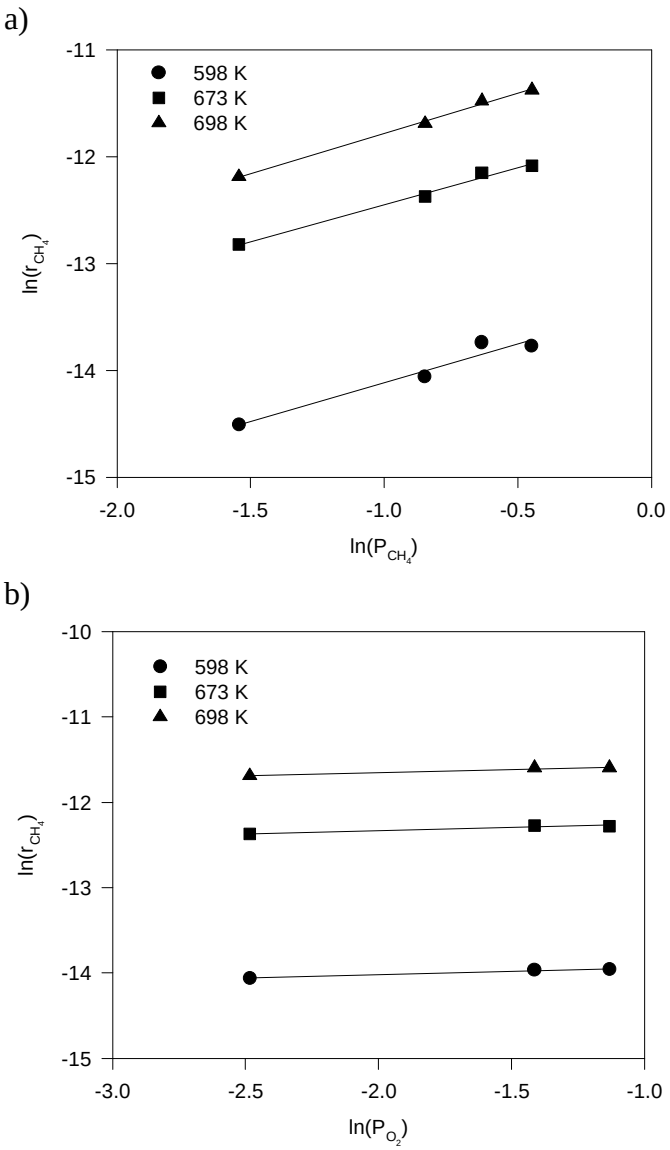

Figure 5-2. Effect of a) methane partial pressure and b) oxygen partial pressure on methane oxidation rate over unpromoted VPO.

Temperature dependence of the rate was determined by varying the temperature between 583 and 713 K. An Arrhenius plot is shown in Figure 5-20 in section 5.3. The linear nature of this plot, even at the highest conversions (in all cases well below 10%) and temperatures confirms the absence of significant mass transfer limitations in this system. An activation energy of 102±6 kJ/mole is calculated for methane conversion.

5.1.4. Reaction Studies: Methanol. The methanol oxidation experiments described here were conducted in the temperature range of 423 to 648 K, gas hourly space velocity (GHSV) of 3,300 to 15,000 h^{-1}, methanol partial pressure of 8.4 to 48.4 kPa, and methanol-to-oxygen ratio of 0.25 to 1.13. The principal products of methanol oxidation over VPO were dimethyl ether, formaldehyde, carbon monoxide and carbon dioxide. Figure 5-3 presents selectivity to these products as a function of conversion, varied by varying temperature and GHSV. Dimethyl ether

and formaldehyde were the only products at low methanol conversion. In the temperature range of 423 to 458 K dimethyl ether was found to be the only product. Above 473 K formaldehyde became the major product in the reactor effluent.

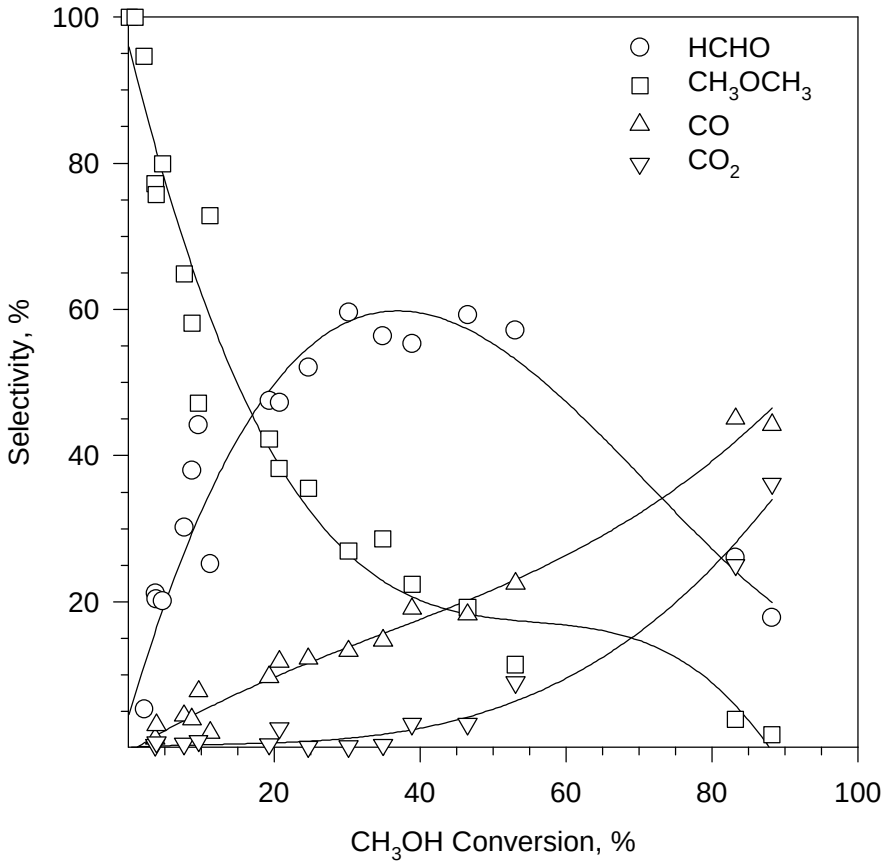

Figure 5-3. Product selectivity as a function of methanol conversion, third order regression curves are for clarity only.

5.1.5. Reaction Studies: DME. Dimethyl ether oxidation over VPO was performed at 438 to 573 K temperature range, GHSV of 6,900 to 12,500 h^{-1}, dimethyl ether partial pressure of 2.2 to 4.9 kPa, and dimethyl ether-to-oxygen ratio of 0.66-1.19 (similar to the conditions used for methanol). Product selectivity as a function of dimethyl ether conversion is given in Figure 5-4. Conversion was varied by varying GHSV and the temperature. Methanol, formaldehyde, carbon monoxide and carbon dioxide were the principal reaction products. Methanol is the primary reaction product at low conversion levels and is converted sequentially to HCHO and CO. Carbon dioxide appears to form directly from dimethyl ether at higher conversion levels given that CO_2 is only a minor product of methanol oxidation (Figure 5-3). Formations of trace levels of higher order products like methyl formate and dimethoxymethane and slightly higher levels of methane have also been observed.

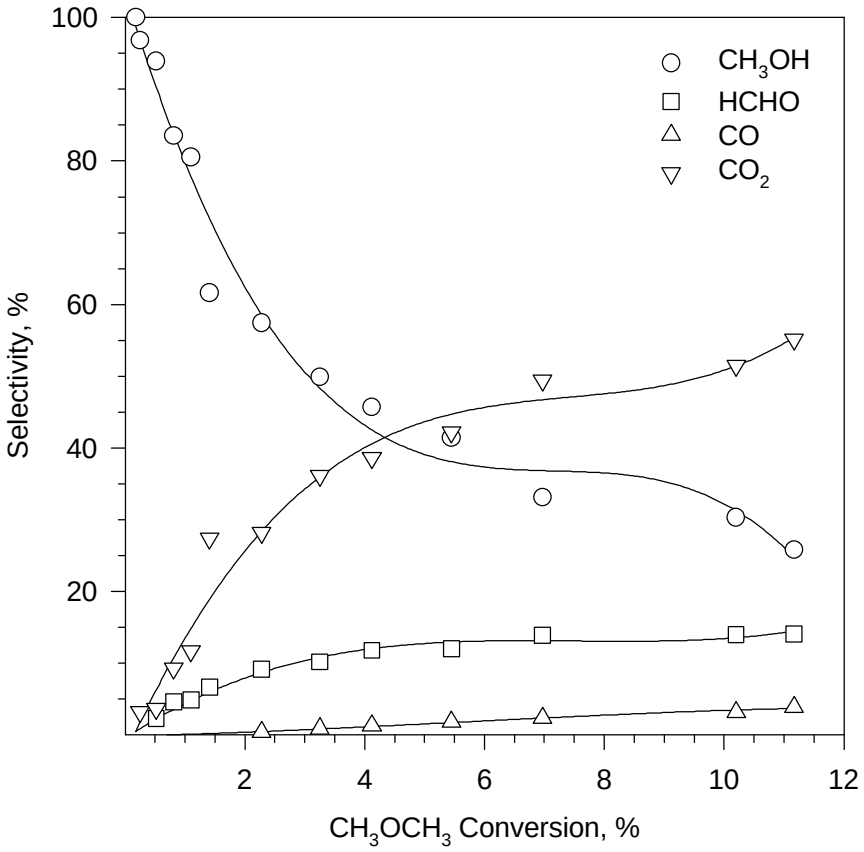

Figure 5-4. Product selectivity as a function of dimethyl ether conversion, third order regression curves are for clarity only.

5.1.6. Reaction Studies: Formaldehyde. The formaldehyde oxidation experiments were conducted in the temperature range of 473-623 K, GHSV of 4,200-12,550 h^{-1}, formaldehyde partial pressures of 2.3-13.5 kPa and formaldehyde-to-oxygen ratio was varied between 0.06-0.2. Carbon monoxide and carbon dioxide are the only significant reaction products. Product selectivity as a function of hydrocarbon conversion is given in Figure 5-5, where the formaldehyde and oxygen partial pressures are constant at a ratio 0.06. At low conversion, carbon monoxide was the only product observed. As the conversion of formaldehyde was increased, carbon monoxide selectivity decreased.

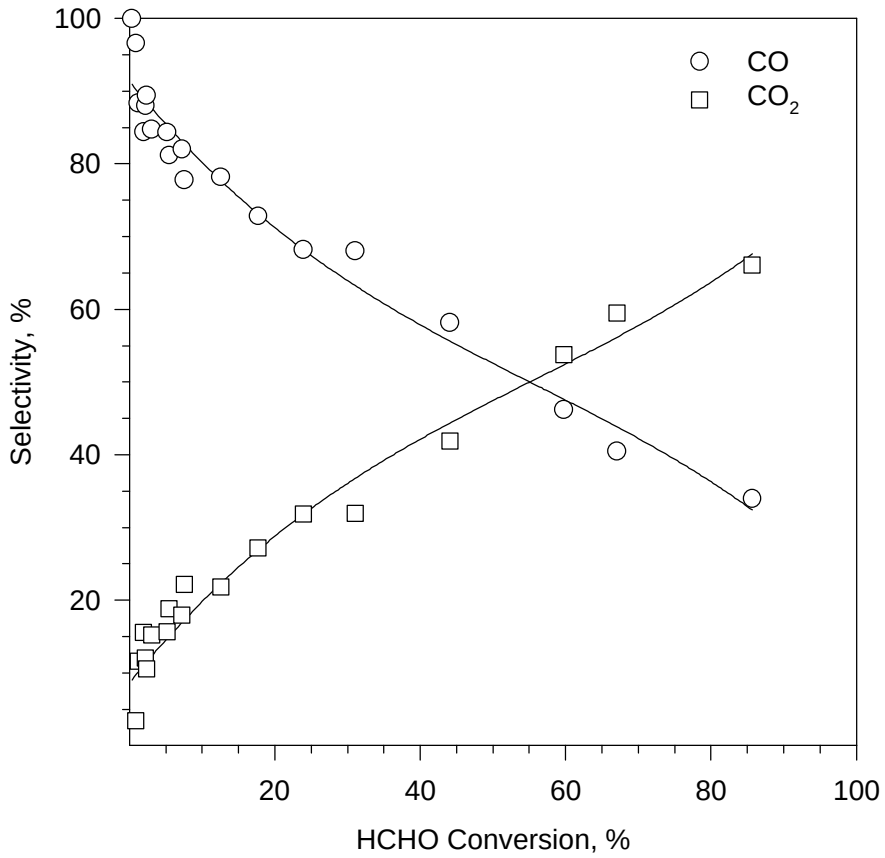

Figure 5-5. Product selectivity as a function of formaldehyde conversion.

5.1.7. Kinetic Analysis for Methanol, DME, and Formaldehyde. The selectivity-conversion pattern reported in Figures 5-3 to 5-5 suggests that methanol is consumed via a parallel reaction path as shown below:

$$2\ CH_3OH \xrightarrow{k_1} (CH_3)_2O + H_2O$$

$$(CH_3)_2O + H_2O \xrightarrow{k_{-1}} 2\ CH_3OH$$

$$CH_3OH + \frac{1}{2}O_2 \xrightarrow{k_2} HCHO + H_2O$$

$$(CH_3)_2O + \frac{3}{2}O_2 \xrightarrow{k_3} 2\ HCHO + H_2O$$

$$(CH_3)_2O + \frac{7}{2}O_2 \xrightarrow{k_4} 2\ CO_2 + 3\ H_2O$$

$$HCHO + \frac{1}{2}O_2 \xrightarrow{k_5} CO + H_2O$$

$$CO + \frac{1}{2}O_2 \xrightarrow{k_6} CO_2$$

Reaction 1 is the reversible dehydration of methanol yielding dimethyl ether and water as the products. In a separate reaction path methanol is partially oxidized into formaldehyde (Reaction

2). Very low selectivity to carbon monoxide and carbon dioxide at low methanol conversion suggests that there is no direct oxidation route from methanol to these species. Dimethyl ether is converted in a more complicated parallel reaction path. The reverse of reaction 1 hydration of dimethyl ether to methanol occurs. The presence of carbon dioxide at low conversion values indicates a direct route from DME to CO_2 (Reaction 4). Since no CO_2 formation is observed at low methanol conversion levels, this species has to form because of DME oxidation. Another reaction route from DME to formaldehyde can also be suggested because significant formaldehyde selectivity (above 10%) is observed even at low DME conversion levels. At higher conversion levels, methanol oxidation into formaldehyde occurs along with methanol dehydration.

Data obtained under differential conditions (conversion of approximately 10% or less) for each reactant was fit to a power law rate model, given by Equation 1:

$$-r_{HC} = k_i P_{HC}^{a} P_{O_2}^{b} \quad \text{..... [1]}$$

α and β are reaction orders for hydrocarbon (methanol, DME, formaldehyde) and oxygen, respectively.

To determine overall reaction orders for the methanol oxidation reaction, methanol partial pressure was changed between 8.8 and 39.4 kPa, keeping the oxygen partial pressure and GHSV constant at 34.5 kPa and 7,500 hr^{-1}, respectively. At the same GHSV, oxygen partial pressure was changed from 8.0 to 39.5 kPa, at a constant methanol partial pressure of 14.2 kPa. Regression analysis yields reaction orders for methanol and oxygen of 1.12 and 0.09, respectively.

Overall reaction orders for the dimethyl ether oxidation reaction were determined in a similar set of experiments at a constant GHSV of 9000 hr^{-1}. Dimethyl ether partial pressure was kept constant 3.9 kPa while oxygen partial pressure was varied from 3.7 to 8.5 kPa. In a separate set of experiments, oxygen partial pressure was kept constant at 3.7 kPa while dimethyl ether partial pressure was varied from 2.4 to 4.2 kPa. The results of the regression analysis indicate the reaction order for dimethyl ether is 1.04. The rate of reaction of dimethyl ether showed a small positive order in oxygen of about 0.04.

To determine reaction orders for formaldehyde oxidation reaction, formaldehyde partial pressure was changed between 2.3 to 13.5 kPa, keeping the oxygen partial pressure constant at 38.5 kPa. During these runs, GHSV was also kept constant at 4200 h^{-1}. In a similar test, oxygen partial pressure was changed from 16.4 to 38.5 kPa, keeping formaldehyde partial pressure constant at 13.5 kPa. A direct proportionality between reaction rate and formaldehyde partial pressure is observed. Product selectivity was not affected by reactant partial pressure. Multiple regression of equation 1 to the data indicates the reaction to be 0.95 order in formaldehyde and 0.06 order in oxygen.

These steady state runs were repeated at different temperatures to observe the effects of temperature on reaction order or to the suggested reaction scheme. Reaction orders were not affected by temperature over the range studied. While global reaction orders have little fundamental meaning for complex reaction networks, the reaction order determination supports

the assumption that all reactions are first order in hydrocarbon and zero order in oxygen in the following analysis.

Based on the reaction scheme suggested above the methanol oxidation system can be modeled in the following form:

$$\frac{dP_{CH_3OH}}{dt} = -k_1 P_{CH_3OH} + - k_2 P_{CH_3OH} + k_{-1} P_{(CH_3)_2O} \quad \text{.....[2]}$$

$$\frac{dP_{(CH_3)_2O}}{dt} = -k_{-1} P_{(CH_3)_2O} - k_3 P_{(CH_3)_2O} - k_4 P_{(CH_3)_2O} + k_1 P_{CH_3OH} \quad \text{.....[3]}$$

$$\frac{dP_{HCHO}}{dt} = -k_5 P_{HCHO} + k_3 P_{(CH_3)_2O} + k_2 P_{CH_3OH} \quad \text{.....[4]}$$

$$\frac{dPc_O}{dt} = k_5 P_{HCHO} - k_6 P_{CO} \quad \text{.....[5]}$$

$$\frac{dPc_{O_2}}{dt} = k_6 P_{CO} + k_4 P_{(CH_3)_2O} \quad \text{.....[6]}$$

Space time, t, is defined as volume of the catalyst bed/total volumetric flowrate at the reactor temperature. With the first order reaction assumption, rate constants will all have the same units (min^{-1}). The assumption of zero order in oxygen should break down when the oxygen concentration becomes very low. This regime was not extensively investigated as the nature of the catalytic surface was thought to change at low oxygen concentration. In order to evaluate the model parameters the results of formaldehyde oxidation experiment were evaluated separately (k_2 and k_3 are zero for these experiments) and the obtained rate parameters were used in calculating related parameters in methanol and DME oxidations.

Reaction rate constants for formaldehyde (k_5) and carbon monoxide (k_6) oxidation reactions were calculated from the data using the numerical quadrature method, described by Gay (1971). A sequential reaction path is indicated for formaldehyde oxidation in which carbon dioxide forms at the expense of carbon monoxide in a consecutive reaction.

$$\begin{aligned} HCHO + \frac{1}{2}O_2 &\xrightarrow{k_5} CO + H_2O \\ CO + \frac{1}{2}O_2 &\xrightarrow{k_6} CO_2 \end{aligned} \quad \text{..... [7]}$$

Determination of k_5 and k_6 requires simultaneous solution of the following differential equations:

$$\frac{dC_{HCHO}}{dt} = -k_5\ C_{HCHO}$$

$$\frac{dC_{CO}}{dt} = k_5\ C_{HCHO} - k_6\ C_{CO} \quad \text{..... [8]}$$

$$\frac{dC_{CO_2}}{dt} = k_6\ C_{CO}$$

Instead of seeking a numerical solution to the differential equations given in Equations 8, the system is simplified by introduction of new variables, the time (or space time) integrals of the various concentrations. Direct integration of equations 8 yields:

$$P_{HCHO} - P_{HCHO}^{\ o} = -k_5 \int_0^t P_{HCHO}\ dt$$

$$P_{CO} - P_{CO}^{\ o} = k_5 \int_0^t P_{HCHO}\ dt - k_6 \int_0^t P_{CO}\ dt \quad \text{..... [9]}$$

P_{HCHO}^{o} and P_{CO}^{o} are the initial concentrations of formaldehyde and carbon monoxide. A numerical value for the integrals is obtained from the partial pressure versus space time data. Then algebraic solution of Equations 9 yields numeric values for k_5 and k_6. Similar experiments were repeated at different temperatures to determine activation energy of these reactions. An Arrhenius plot is given in Figure 5-6 from which the activation energies for formaldehyde and carbon monoxide oxidation were determined. Rate constants and activation energies of formaldehyde and carbon monoxide oxidation reactions are given in Table 5-1.

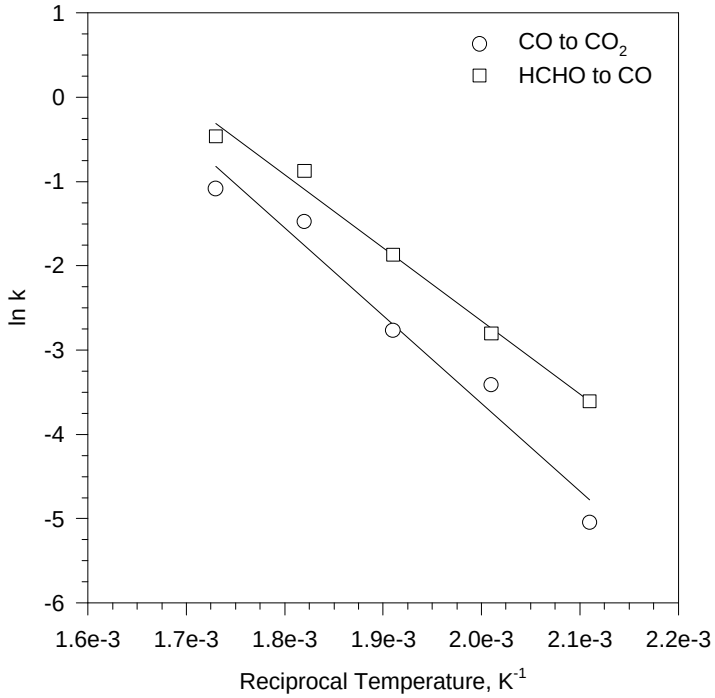

Figure 5-6. Arrhenius plot for formaldehyde and carbon monoxide oxidation reactions.

For the given set of consecutive reactions the product selectivity for carbon monoxide and carbon dioxide can be defined as:

$$S_{CO} = \frac{P_{CO}}{P_{HCHO}^{o}}$$

$$S_{CO_2} = \frac{P_{CO_2}}{P_{HCHO}^{o}} \quad \text{.....[10]}$$

Dividing the mass balance equations for CO and CO_2 (Equations 5 and 6 with k_4 equal to zero) by the equation for HCHO (Equation 4 with k_2 and k_3 equal to zero):

$$\frac{dP_{CO}}{dP_{HCHO}} = -1 + \frac{k_6 \; P_{CO}}{k_5 \; P_{HCHO}} \quad \text{.....[11]}$$

$$\frac{dP_{CO_2}}{dP_{HCHO}} = -\frac{k_6 \; P_{CO}}{k_5 \; P_{HCHO}} \quad \text{.....[12]}$$

Since Equations 11 and 12 are linear, first order differential equations, an analytical solution can be obtained:

$$S_{CO} = \frac{P_{CO}}{P_{HCHO}^{o}} = \frac{k_5}{k_5 - k_6}\left\{\left(\frac{P_{HCHO}}{P_{HCHO}^{o}}\right)^{\frac{k_6}{k_5}} - \frac{P_{HCHO}}{P_{HCHO}^{o}}\right\} \quad \text{.....} \quad [13]$$

$$S_{CO_2} = \frac{P_{CO_2}}{P_{HCHO}^{o}} = \frac{k_5}{k_5 - k_6}\left\{1 - \left(\frac{P_{HCHO}}{P_{HCHO}^{o}}\right)^{\frac{k_6}{k_5}}\right\} - \frac{k_6}{k_5 - k_6}\left(1 - \frac{P_{HCHO}}{P_{HCHO}^{o}}\right) \quad \text{.....} \quad [14]$$

where S denotes the overall selectivity.

Using these selectivity relationships, predicted selectivity is compared with observed values for carbon monoxide and carbon dioxide in Figure 5-7. The mathematical model, built on the assumption that the reaction rate is zero order in oxygen and first order in formaldehyde concentration, is also compared to experimentally observed rate values in Figure 5-7. Model predictions compare well with the experimental observations.

The results obtained from formaldehyde oxidation (values of k_5 and k_6) were then used to solve the set of differential equations given in Equations 1 through 3 using the numerical quadrature approach. These three differential equations involve five more unknowns k_1, k_{-1}, k_2, k_3, k_4. Additional relationships were provided by applying numerical quadrature technique to the dimethyl ether oxidation (to relate k_3 and k_4) and in the form of thermodynamic data for the methanol dehydration reaction. Standard free energies of formation for CH_3OH and $(CH_3)_2O$ are 161.4 and 108.9 kJ/mole, respectively. The methanol dehydration reaction to dimethyl ether is endothermic (ΔH_R^o =19.64 kJ/mole) and thus the equilibrium constant (k_1/k_{-1}) increases with the temperature. In the temperature range employed in this study (423 to 648 K) the equilibrium constant was less than 1. Thus methanol was the thermodynamically more favorable product and

high DME yields are not expected. Partial pressure data as a function of space time were collected at different temperatures which allows us to draw the Arrhenius plot given in Figure 5-8 and obtain activation energy for these reactions. The calculated results are tabulated in Table 5-1.

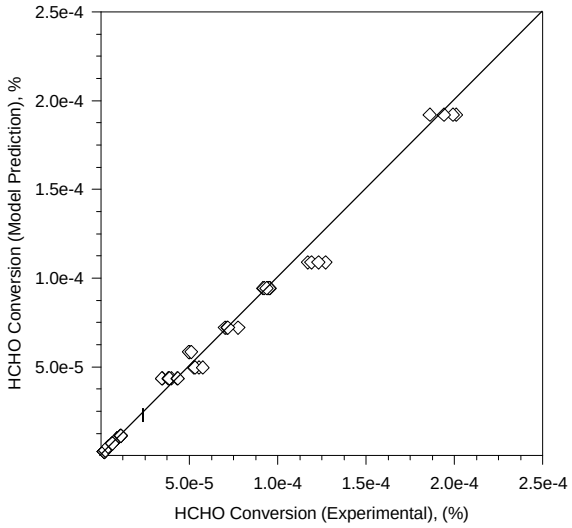

a)

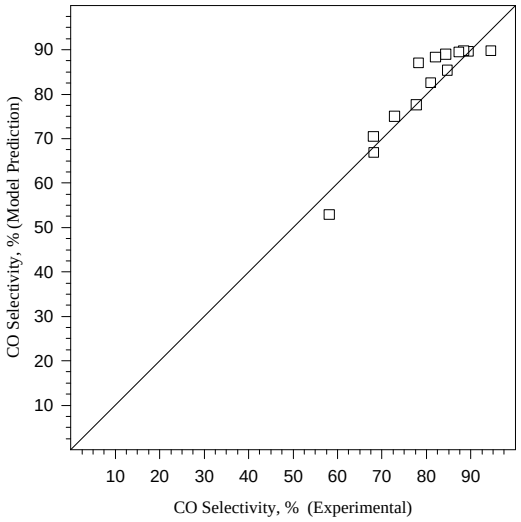

b)

Figure 5-7. Comparison of experimental and model-calculated a) rate of formaldehyde oxidation and b) CO selectivity.

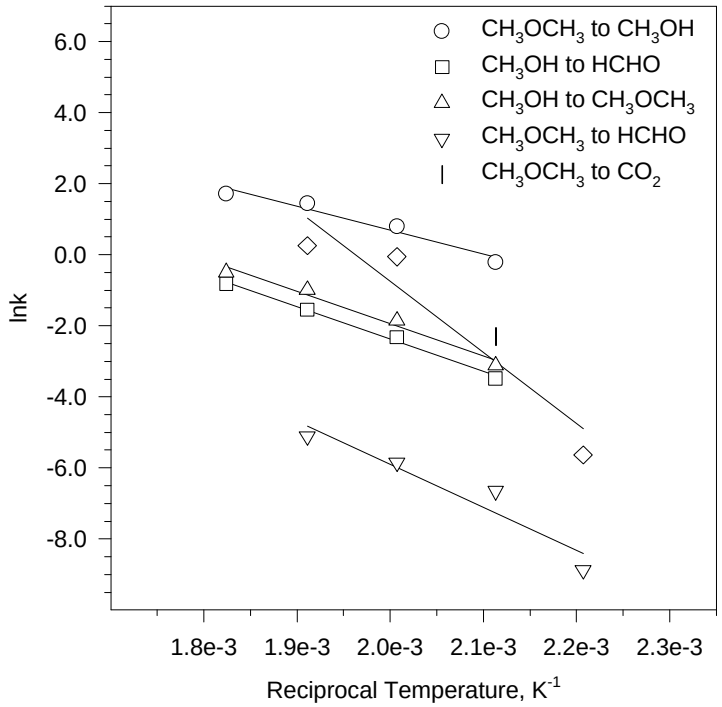

Figure 5-8. Arrhenius plot for methanol, dimethyl ether oxidation/hydration reactions.

Table 5-1. Kinetic Parameters of Methanol, Dimethyl Ether and Formaldehyde Oxidation/Hydration Reactions.

Reaction	**Rate Constant at 473 K (min^{-1})**	**Activation Energy (kJ/mole)**	**Preexponential Factor (min^{-1})**
$CH_3OH \rightarrow HCHO$	0.034	76	$8.37x10^6$
$CH_3OH \rightarrow DME$	0.064	75	$1.22x10^7$
$DME \rightarrow CH_3OH$	0.974	56	$1.49x10^6$
$DME \rightarrow HCHO$	0.001	101	$9.89x10^7$
$DME \rightarrow CO_2$	0.510	59	$1.67x10^6$
$HCHO \rightarrow CO$	0.027	72	$2.37x10^6$
$CO \rightarrow CO_2$	0.009	86	$2.83x10^7$

Comparison of experimental and predicted methanol conversion is shown in Figure 5-9. The rate model and parameters over predict methanol conversion at high conversion levels. The failure of our model to accurately predict methanol conversion is most likely due to the inhibiting effect of water (Holstein and Machiels, 1996).

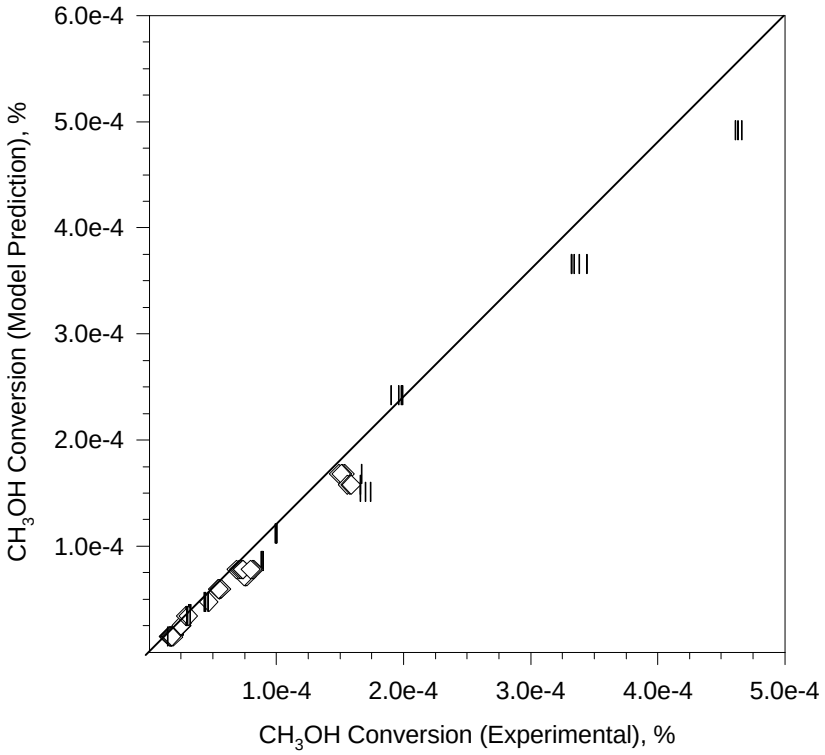

Figure 5-9. Comparison of experimental methanol conversion rate with model predictions.

The results reported demonstrate that vanadyl pyrophosphate is an active catalyst for oxidation of methanol, dimethyl ether, and formaldehyde. Methanol is primarily converted to formaldehyde under the conditions employed here. DME is converted to methanol and formaldehyde, as well as directly to carbon dioxide. Formaldehyde oxidation is facile producing carbon dioxide.

5.2. Modification of the Surface Acidity of $(VO)_2P_2O_7$

Strong Lewis acid sites have been observed on the surface of VPO and are thought to be responsible for initial alkane activation (Busca, et al., 1986b). It has been proposed that this Lewis acidity is related to lattice defects or strain initiated by disorder in the stacking of the layered structure (Busca, et al., 1986b; Horowitz, et al., 1988) as evidenced by broadening of the (200) reflection in the x-ray powder pattern. However, equilibrated catalysts (used for at least 200 hours) exhibit a lower degree of structural disorder, but a higher level of strong Lewis acidity compared to freshly activated catalysts (Cornaglia, et al., 1993b). Thus the structural disorder is not itself a cause of the strong acid sites but may be a secondary effect of the same factors that generate strong acidity during catalyst preparation. In this section we describe procedures we have employed to increase the acid site density of vanadyl pyrophosphate and the effect of increased acidity on methane conversion and selectivity. We have attempted to increase the acidity (site density and strength) of vanadyl pyrophosphate by modifying the preparation procedure. We examine two modifications to the basic preparation procedure which enhance disorder in the layer stacking and the effect of these modifications on surface acidity. For comparison a sample where the acidic protons were exchanged for potassium was also prepared.

5.2.1. Catalyst Synthesis. Vanadyl pyrophosphate (Catalyst A) was prepared in a solution of iso-butyl and benyl alcohols after Busca and coworkers (1986a). A novel preparation was performed by replacing the benzyl alcohol with its two ring analog, naphthalene methanol and using procedures identical to those above (Catalyst B). By using a larger molecule, naphthalene methanol, we hoped to enhance any disorder caused by trapping of organic molecules in the precursor structure and any consequent acidity generation. Vanadyl pyrophosphate modified by addition of tetraethyl orthosilicate (TEOS, Catalyst C) was prepared after Horowitz and coworkers (1988) who demonstrated that this procedure produced additional structural disorder and might therefore affect surface acidity. Conversion of the dried (423 K in air, overnight) catalyst precursors to the active phase was performed in ceramic boats placed in a quartz tube furnace under a stream of air or 1.5% butane in air. The temperature was gradually increased from room temperature through 398 K (40 min.), 623 K (40 min.) and finally 673 K where it was held for 24 hours. Catalyst A, after activation, was impregnated with a solution of potassium acetate in anhydrous ethanol (Catalyst D). The estimated potassium loading after this incipient wetness procedure was 1 weight percent. This sample was dried overnight and further activated in the butane air mixture at 673 K for 5 hours.

5.2.2. Catalyst Characterization. Surface areas for the catalysts are listed in Table 5-2. Both modified preparations (Catalysts B and C) have significantly reduced surface area relative to Catalyst A. X-ray diffraction results for the three catalyst precursors are shown in Figure 5-10. Modification by addition of TEOS (Catalyst C) results in a large reduction in the relative intensity of the (001) reflection, indicative of disorder in the direction perpendicular to the layer plane (Busca, et al., 1986b). Substitution of naphthalene methanol for benzyl alcohol (Catalyst B) produces an amorphous precursor. Thus both modifications were successful at introducing structural disorder. Diffraction data on the activated samples are shown in Figure 5-11. In activated materials the (200) reflection is from the direction perpendicular to the layer plane (4). Both Catalysts B and C exhibit a reduction in the intensity and broadening of this reflection relative to Catalyst A. Peak widths at half maximum listed in Table 5-2 confirm this conclusion. These results show that structural disorder introduced into the precursor by modification of the preparation method persists in the freshly activated catalyst. Thus both modifications to the basic preparation procedure have resulted in enhanced disorder. Chemical analysis indicated that all samples had a bulk P:V ratio in the 0.95-0.98 range.

Table 5-2. Results of catalyst characterization for acidity modification study.

Catalyst	**Surface Area, m^2/g**	**XRD FWHM (020)**	**Bronsted/Lewis Ratio (1540/1447)**	**Methanol Conversion E_a, kcal/mole**
Unmodified (A)	33.1	1.5	2.1	16
Naphthalene Methanol (B)	14.7	1.6	2.8	15
TEOS (C)	20.0	1.7	2.3	20
Potassium Exchange (D)	29.2	--	≈0	10

*Catalyst D contained 1.3 weight percent potassium.

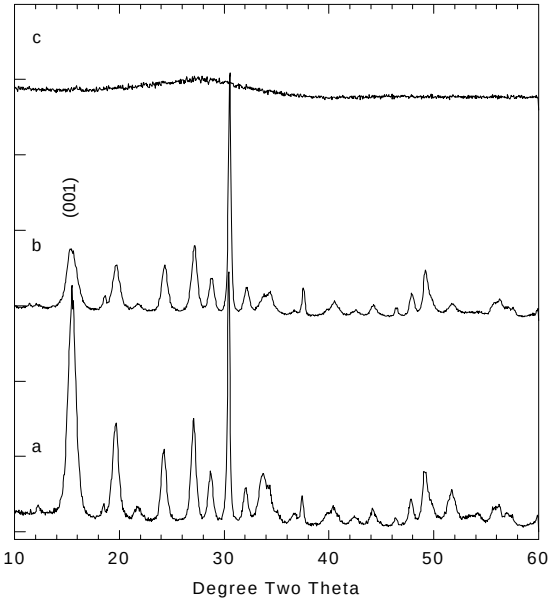

Figure 5-10. X-ray powder diffraction results for catalyst precursors: a) $VOHPO_4$-$0.5H_2O$ prepared in benzyl/isobutyl alcohols, b) similar catalyst modified by addition of TEOS, c) similar catalyst with naphthalene methanol replacing benzyl alcohol.

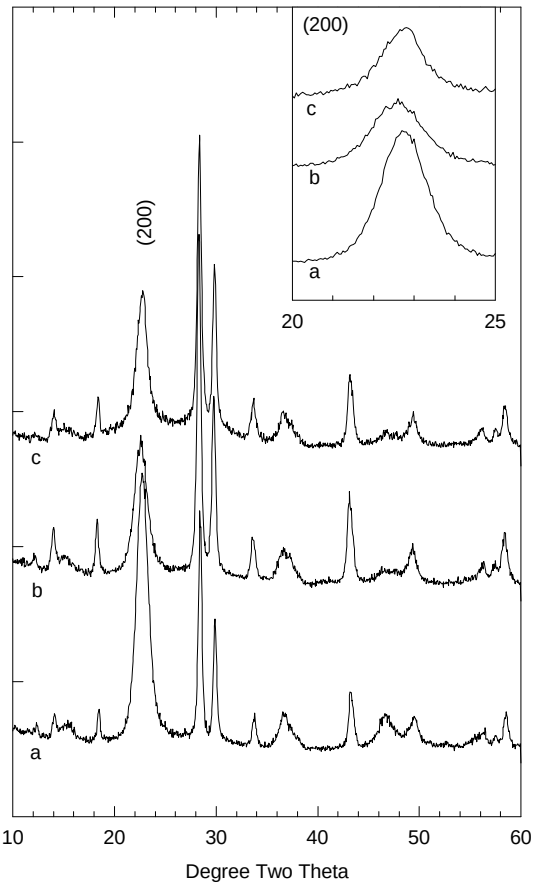

Figure 5-11. X-ray powder diffraction results for activated catalysts: a) $(VO)_2P_2O_7$ activated in air, b) similar catalyst activated in butane/air, c) TEOS modified catalyst activated in butane/air, d) naphthalene methanol preparation activated in butane/air.

Infrared spectra of catalyst precursors prepared by the standard method, with addition of TEOS, and with naphthalene methanol as one of the solvents are shown in Figure 5-12 for the 1800-1400 cm^{-1} region. All samples exhibit the strong peak at 1645 cm^{-1} typical of the in-plane deformation of coordinated water. This is in agreement with the chemical formula of the precursors, $VOHPO_4 \cdot 0.5H_2O$. The conventionally prepared and TEOS catalysts (isobutyl and benzyl alcohol solvents) exhibit bands at 1453 and 1496 from residual benzyl alcohol phenyl ring vibrations. In the preparation where naphthalene methanol was substituted for benzyl alcohol these bands are not present. Instead a number of weak bands can be seen between 1600 and 1500 cm^{-1}, probably characteristic of naphthalene ring vibrations. A relatively strong band is observed at 1684 cm^{-1}, perhaps a C-O stretch. Thus, these vibrational bands may be characteristic of residual naphthalene structures. If so, then we would expect the layer stacking to be more disordered in this material because of the larger size of the trapped organic molecules.

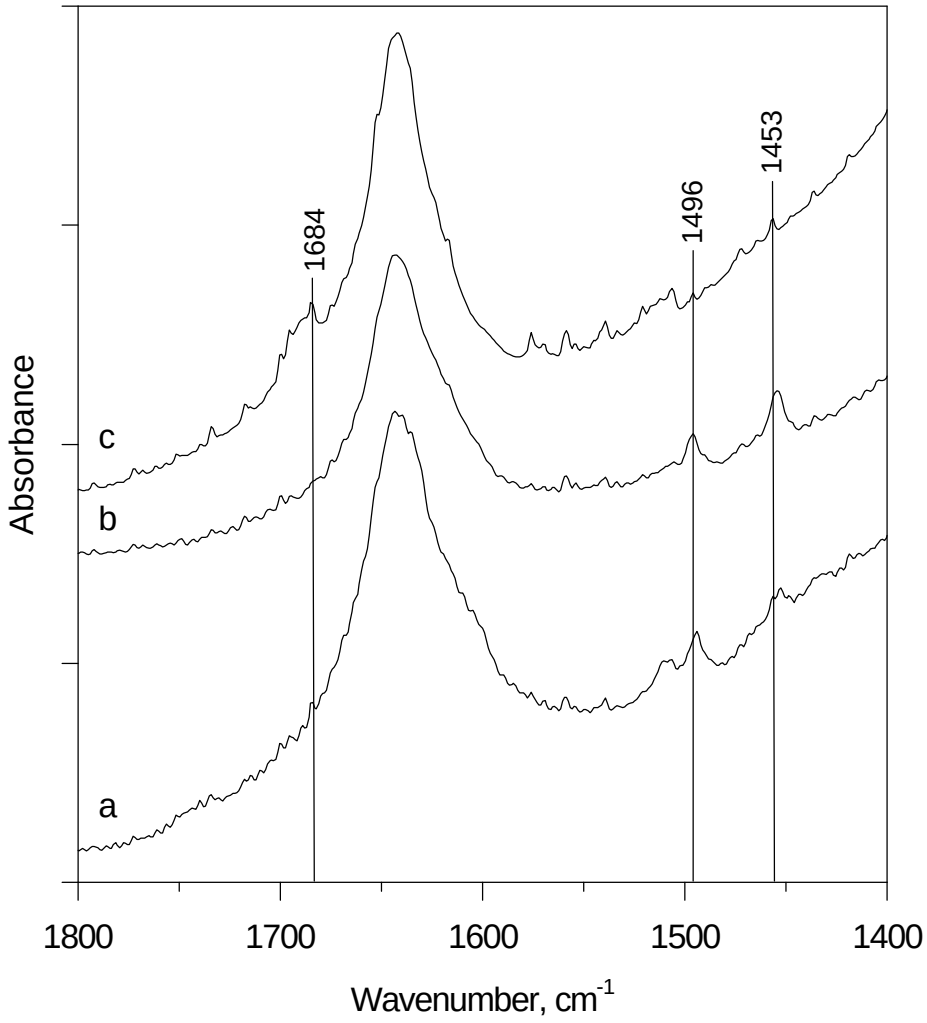

Figure 5-12. Infrared spectra (transmission, KBr pellets) of catalyst precursors: a)conventional organic preparation, b)TEOS modification, c)naphthalene methanol as a solvent.

These catalysts have also been characterized by infrared spectroscopy (diffuse reflectance) of chemisorbed pyridine and acetonitrile. The purpose of these studies was to determine if preparation method modifications had resulted in increased surface acid site strength or other changes in the nature of the surface acidity. All catalysts exhibited peaks characteristic of pyridine chemisorbed on both Bronsted (1640 and 1542 cm^{-1}) and Lewis (1612, 1578, 1490, and 1450 cm^{-1}) acid sites. The position of the ν(8a) vibration (1578 cm^{-1} in the liquid) is sometimes employed to measure the strength of the Lewis sites. For the four catalysts tested here the position of this band ranges from 1609 to 1612 indicating little significant difference in Lewis site strength as determined by pyridine adsorption. It is apparent that doping of the surface with potassium has resulted in a dramatic decrease in the relative intensity of bands for adsorbed pyridinium ion (1640 and 1542 cm^{-1}) confirming the removal of most of the Bronsted acid sites on this sample. Bronsted to Lewis site ratios were estimated from the integrated intensity of the IR bands at 1540 cm^{-1} (Bronsted) and 1447 cm^{-1} (Lewis). This procedure ignores differences in the extinction coefficient for pyridine on the two different types of sites but should provide a

reasonable basis for comparison of the catalysts studied here. The Bronsted/Lewis ratios for Catalysts A, B, and C are essentially identical as shown in Table 5-2.

5.2.3. Reaction Studies: Methanol and Methane. The activity of these catalysts for methanol dehydration was examined in the temperature range of 423 to 493 K, GHSV of 10,400 h^{-1}, and inlet gas partial pressures of 0.21 atm O_2, 0.12 atm CH_3OH, balance He. Under these conditions conversion was between 0 and 3 percent and DME was by the dominant reaction product. Figure 5-13 shows catalyst activity for methanol coupling as a function of temperature. The measure of activity is the observed reaction rate on either a catalyst mass or surface area basis. In both cases the TEOS modified material is the most active catalyst. However, on a surface area basis the naphthalene methanol modified catalyst is more active than the unmodified material, a switch in relative activity from the mass basis comparison.

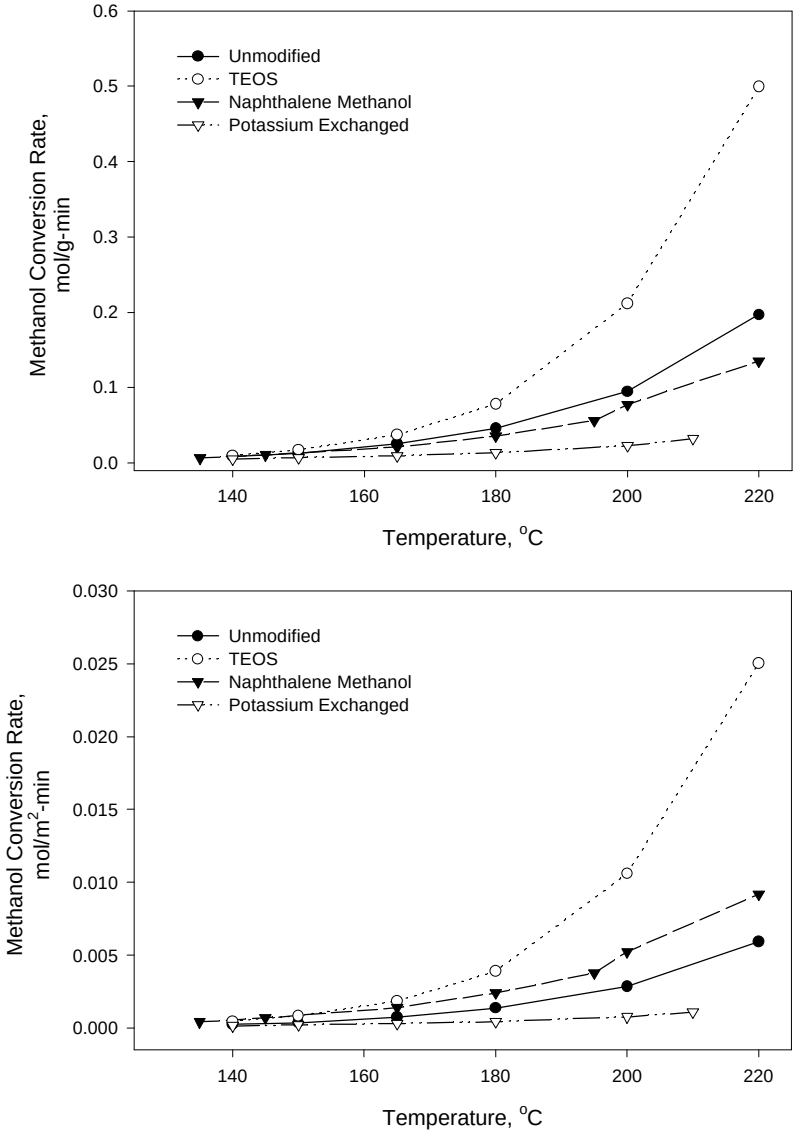

Figure 5-13. Activity of surface acidity modified materials for methanol conversion on a mass (top) and surface area (bottom) basis.

Thus, both methods of acidity modification were successful at increasing catalyst activity in an acid catalyzed reaction, dehydration of methanol. As expected, poisoning of the acid sites with potassium significantly reduces activity. Arrhenius plots (not shown) yield the activation energies listed in Table 5-2. There is not difference in activation energy between the unmodified and the naphthalene methanol modified catalysts for methanol conversion. For the TEOS modification the activation energy is apparently larger, however these values are probably identical with in the error of this particular data set. Thus we must conclude that both attempts at acidity modification resulted in more acid sites per unit surface, not in stronger sites.

Methane oxidation experiments were performed to determine if the catalyst modifications attempted in this work resulted in enhanced activity for activation of the methane C-H bond. These experiments were conducted at very low conversions (differential reactor) and with a large excess of methane relative to oxygen (CH_4:O_2 molar ratio of 25:1). Oxygen conversions were always less than 50%. Gas hourly space velocities ranged from 1400 to 2400 hr^{-1}. Under these conditions the only reaction product observed was carbon monoxide. By measuring methane conversion at several temperatures over these catalysts and making the assumptions of a differential reactor and first order reaction kinetics for methane, the catalysts can be compared on the basis of apparent first order rate constants. These rate constants are compared in Figure 5-14. The naphthalene methanol catalyst has a similar level of activity to the unmodified catalyst, although only two data points are available. The catalyst modified through addition of TEOS has lower activity. The rate constants are based on reaction rates per gram of catalyst. Thus it is again apparent that acid strength was unchanged by the catalyst modifications.

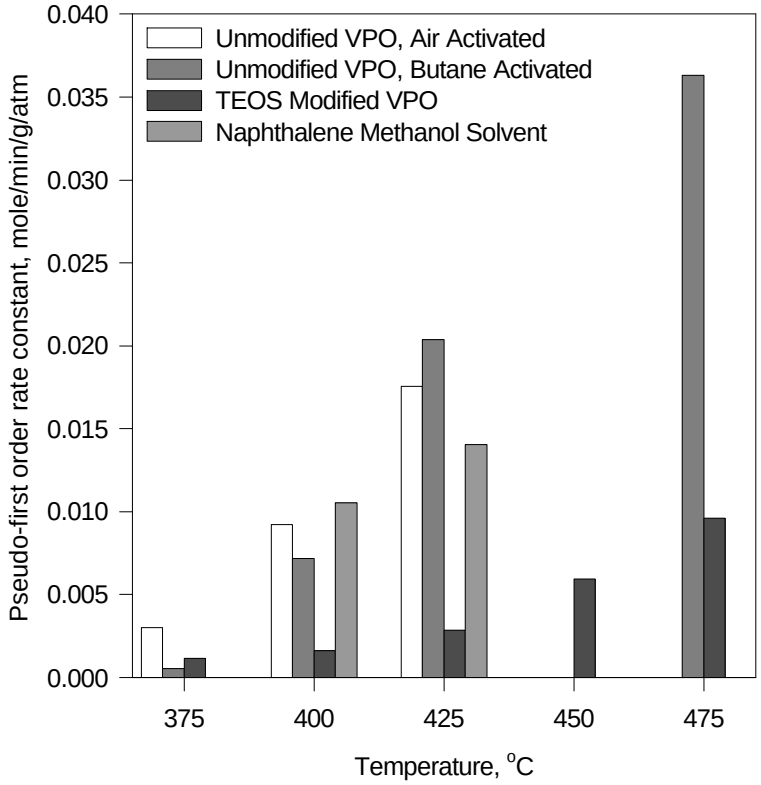

Figure 5-14. Apparent first order rate constants for methane conversion over catalysts from acidity modification study.

5.3. Promotion of $(VO)_2P_2O_7$ by Fe and Cr

A variety of cations have been added to vanadium phosphate catalysts to improve catalyst activity or selectivity (Hutchings, 1991). For n-butane oxidation beneficial effects have been claimed for promotion by many of the first row transition metals (Hutchings, 1991; Otake, 1982; Takita, et al., 1993; Hutchings and Higgins, 1996; Sananes-Schulz, et al., 1996). Vanadyl pyrophosphate promoted with Fe and Cr has been examined for the methane partial oxidation reaction in this work.

5.3.1. Catalyst Synthesis. Nitrate salts of Cr and Fe were used as the source of promoter elements. Five grams of Cr^{III} nitrate nonahydrate or 5.05 g of Fe^{III} nitrate nonahydrate was dissolved in a benzyl/isobutyl alcohol mixture. This was then added to 45 g of previously prepared precursor(prepared as described in Section 5.1.1) that had been resuspended under reflux in a benzyl/isobutyl alcohol mixture and cooled. This mixture was then stirred at 323 K overnight. The precipitate was then filtered and washed with more solvent, and dried in a rotary vacuum drier for 8 hours at slightly greater than ambient temperature. The promoted catalyst precursors were activated in the same way described for unpromoted VPO.

5.3.2. Catalyst Characterization. X-ray diffraction data obtained for the precursor show the peaks of vanadyl phosphate hemihydrate $VOHPO_4$-$0.5H_2O$. A poorly crystalline vanadyl pyrophosphate was the only phase observed by XRD in the activated, unpromoted sample as shown in Figure 5-15. Given the broadness of some of the XRD peaks, the presence of other VPO phases cannot be completely ruled out, however. After exposure to methane oxidation conditions for 20 hours the (200) reflection at 22.8° has increased in intensity, suggesting that order in the layer stacking direction has increased.

Figure 5-15 also reports X-ray diffraction data for both transition metal promoted VPO catalysts after activation and after use for 20 hours in methane oxidation. These data show that additional peaks are evident for Fe and Cr promoted VPO. In the Cr-promoted sample, peaks at 24.9° (3.58 Å), 29.15° (3.06 Å) and 40.71° (2.21Å) in the activated sample correspond to α_{II}-$VOPO_4$ (Ben Abdelouahab, et al., 1992). The peak at 12.2° (7.26 Å) could not be assigned. These are reduced in intensity after exposure to methane oxidation conditions and a new peak is observed at 21.9° (4.21 Å). The crystallinity of this material does not appear to have developed during catalysis, as relative peak intensities are essentially unchanged. These data indicate that addition of Cr by the method outlined in the experimental section causes the predominantly vanadyl pyrophosphate starting material to be oxidized. For the Fe-promoted sample, peaks at 27.1° (3.29 Å) and 30.4° (2.94 Å) after activation do not correspond to obvious oxide phases of the promoter or of V-P-O. These peaks might correspond to iron phosphates but with only two peaks a definitive assignment cannot be made. After exposure to methane oxidation conditions peaks corresponding to a $VOPO_4$ phase are observed at 25.8° (3.95 Å), 29.2° (3.06 Å), and 40.7° (2.24 Å). It is notable that the (200) reflection at 22.8° is much more intense in this catalyst following activation than in the others. After use in methane/oxygen the relative intensity is comparable to that for the unpromoted VPO. These data indicate that Fe promotion enhances the rate of development of crystallinity, and suggest that one reason for the use of Fe as a promoter

for industrial butane oxidation catalysts (Hutchings, 1991) is because equilibrium catalysts are more rapidly obtained.

Surface areas are listed in Table 5-3 and are nearly identical for all three catalysts. XPS results, also in Table 5-3, indicate that roughly one tenth of the surface metal atoms are promoter. Bulk analysis yields similar results indicating that the method of introducing promoters modifies both the surface and bulk composition. Surface P:V ratios are well above 1.0 as has been reported for commercial butane oxidation catalysts. Bulk P:V ratios are slightly below 1.0 and slightly below the ratio employed in the catalyst synthesis.

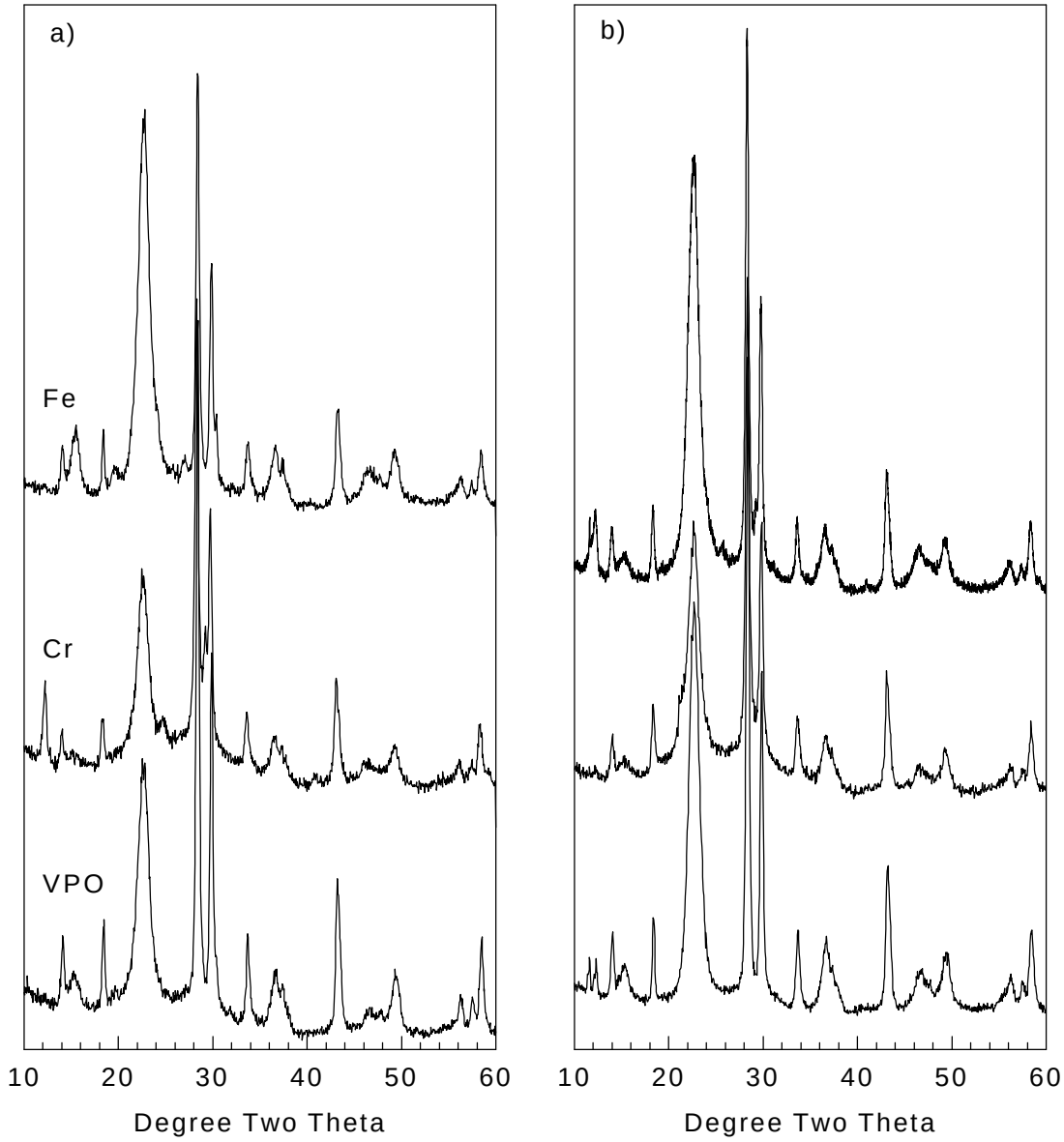

Figure 5-15. X-ray diffraction patterns of unpromoted and promoted vanadyl pyrophosphate catalysts: a) freshly activated in butane/air, b) after 20 hours use in methane oxidation.

Table 5-3. Characterization results for vanadyl pyrophosphate and promoted catalysts.

Catalyst	Surface Area (m^2/g)	Surface Promoter:V	Bulk Promoter :V	Surface P:V Ratio	Bulk P:V Ratio
VPO	32.1	--	--	1.23	0.97
Cr-VPO	33.8	0.13	0.08	1.58	0.99
Fe-VPO	32.6	0.09	0.11	1.16	0.92

XPS binding energies for vanadium ($2p_{3/2}$), phosphorus (2p), oxygen (1s), and the promoter atoms are listed in Table 5-4. Reported binding energies in the vanadyl pyrophosphate phase (P/V=1.0-1.2) range from 516.6 to 517.9 eV (Cornaglia and Lombardo, 1995; Moser and Schrader, 1987). For reference, V^V compounds show binding energies of 518.2 eV for β-$VOPO_4$ (21) and 517.1 eV for V_2O_5. The binding energy of 516.9 eV reported in Table 5-4 is in good agreement with literature values when differences in the C 1s reference binding energy are considered. Binding energies in this range were also observed for the promoted catalysts although peaks are significantly broadened. Deconvolution of the V $2p_{3/2}$ peak envelope leads to the average vanadium oxidation state reported in Table 5-4. Promotion has resulted in oxidation of a significant fraction of the surface vanadium atoms.

Table 5-4. XPS binding energies and estimated average vanadium oxidation state[a] observed for promoted and unpromoted catalysts.

Catalyst	V $2p_{3/2}$	O 1s	P 2p	$\Delta_{O\ 1s\ -V\ 2p}$	$V_{ox\text{-}Fit}$	$V_{ox\text{-}Corr}$	$V_{ox\text{-}NMR}$
$(VO)_2P_2O_7$	516.5 (1.9)[b]	532.0 (2.2)	134.1 (1.9)	15.1	4.15	3.55	4.03/4.06
Cr-VPO	517.5 (1.8)	531.4 (1.6)	134.0 (1.8)	13.9	4.22	4.38	4.12/4.12
Fe-VPO	517.4 (2.4)	531.3 (1.8)	134.0 (1.8)	13.9	4.38	4.38	4.00/4.10

[a] $V_{ox\text{-}Fit}$ is by the deconvolution approach described in the experimental section. $V_{ox\text{-}Corr}$ is based on the correlation with $\Delta_{O\ 1s\ -V\ 2p}$ presented in Coulston, et al., 1996. $V_{ox\text{-}NMR}$ is based on integration of the ^{31}P NMR intensities after activation/and after catalysis of methane oxidation.

An additional method for discerning vanadium oxidation states employs the difference in binding energy of the O 1s and V $2p_{3/2}$ signals ($\Delta_{O\ 1s\ -\ V\ 2p}$) which is correlated with the surface oxidation states (Cornaglia and Lombardo, 1995; Garbassi, et al., 1986; Coulston, et al., 1996). This approach eliminates the need for a reference binding energy such as C 1s. The binding energy difference for pure vanadyl pyrophosphate, known to contain mostly V^{IV}, varies from 14.9 to 15.2 for P/V=1.0 to 1.2. For the V^V containing β-$VOPO_4$ the binding energy difference is between 13.0 to 13.9 and for V_2O_5 is 12.9 eV. This binding energy difference shifts towards lower energy values with addition of promoter elements consistent with an increase in the amount of V^V on the surface. Coulston and coworkers (1996) present a correlation vanadium average oxidation state and $\Delta_{O\ 1s\ -\ V\ 2p}$. This correlation has also been used to estimate the average vanadium oxidation state and these values are reported in Table 5-4 for comparison with estimates based on deconvolution. The correlated value for the unpromoted catalysts is significantly lower than estimated by our deconvolution approach, and the values for the promoted catalysts are slightly higher. This approach again confirms the difference in average surface oxidation state for the promoted and unpromoted materials.

The $(VO)_2P_2O_7$ phase reported in the literature (Moser and Schrader, 1987) yields an O 1s binding energy of 531.1 to 532.8 eV with a narrow signal (FWHM 2.4 eV). More oxidized V^V phases with and without phosphorous exhibit a much narrower O 1s signals (1.7-2.0 eV), shifted slightly downwards in some cases 531.2 (β-$VOPO_4$) and 530.0 eV (V_2O_5). The data in Table 5-4 indicate O 1s binding energies comparable to pure $(VO)_2P_2O_7$ for the unpromoted as well the Fe and Cr promoted catalysts. The signal is significantly narrower for the promoted materials consistent with a higher average surface oxidation state for vanadium.

Binding energies for the promoter elements were also examined by XPS. For the Fe-promoted catalyst, the Fe $2p_{3/2}$ binding energy value of 714.2 eV indicates very little possibility of presence of FeO or Fe_2O_3 on the surface. The Fe $2p_{3/2}$ energy is 709.5 eV for FeO, 710.8 eV for Fe_2O_3 and 711.5 eV for $FeCl_3$. For Fe promoted vanadyl pyrophosphate the binding energy is much greater. Wang and Otsuka (1995) report a similarly high binding energy of 713.2 eV for $FePO_4$ suggesting the presence of Fe^{III} in a phosphate matrix in the Fe promoted sample. For Cr_2O_3, the $2p_{3/2}$ energy is reported as 576.8 eV. The observed Cr $2p_{3/2}$ energy of 578.3 eV for the Cr-promoted catalyst is very close to the value of 578.5 reported for β-$CrPO_4$ (Watson, et al., 1991), indicating Cr^{III} in a phosphate matrix.

Li and coworkers (1991) introduced the use of ^{31}P NMR spin-echo mapping to determine the presence of bulk V^{IV} and V^V species in vanadium phosphate catalysts. These spectra are characterized by a broad peak centered at about 2500 ppm (relative to H_3PO_4), and assigned to phosphorus in the vicinity of V^{IV}, and a narrower peak near 0 ppm assigned to phosphorus near V^V. Spectra of promoted and unpromoted samples, both freshly activated and after use in methane oxidation, are shown in Figure 5-16. For the activated, unpromoted catalyst there is a small peak for V^V but 97% of the spectral intensity is in the V^{IV} peak at 2500 ppm. Promotion with Cr leads to an increase in the fraction of V^V, which amounts to 12% of the signal intensity. Promotion with Fe produces a sample with essentially no V^V after activation. After use in methane oxidation, the unpromoted and Fe-promoted samples exhibit increased V^V signals, 6% for unpromoted and 10% of signal intensity for Fe-promoted. The spectrum of the Cr-promoted sample is essentially unchanged at 12% V^V. Average vanadium oxidation state estimated by integration of the NMR peak intensities are reported in Table 5-4 for comparison with XPS values. The NMR (bulk) values are slightly lower than the XPS (surface) values determined using the deconvolution approach. However, the results are consistent with the XPS and XRD data, which indicate that promoters enhance the concentration of V^V or oxidized VPO phases, even under the highly reducing conditions employed for methane oxidation.

Diffuse reflectance infrared spectra were obtained for both promoted and unpromoted catalysts. Band positions in the 700 to 1700 cm^{-1} range agreed closely with those reported by others for vanadyl pyrophosphate (Lopez Granados, et al., 1993; Busca, et al., 1986a) with an absorbance maximum at 975 cm^{-1} assigned to V=O stretching. This intense band was broad and not well resolved in these samples. The only significant differences observed in the spectra are for vibrations of the linkages between the layers of the $(VO)_2P_2O_7$ structure and this region of the spectrum is shown in Figure 5-17. For the Cr and Fe promoted catalysts the (V=O)-V band at 795 cm^{-1} has a greater intensity relative to the P-O-P band at 742 cm^{-1} than is observed in the unpromoted catalyst. Examination of the entire infrared spectrum suggests that the band at 742 cm^{-1}, corresponding to the P-O-P stretch, has decreased in intensity. Thus the promoter atoms

are somehow affecting the layer linkages, perhaps by becoming intercalated between the layers. This intercalation, if it occurs, does not appear to have produced disorder in the layer stacking as shown by XRD. Ordering and crystallinity may have actually increased for the Fe-promoted sample.

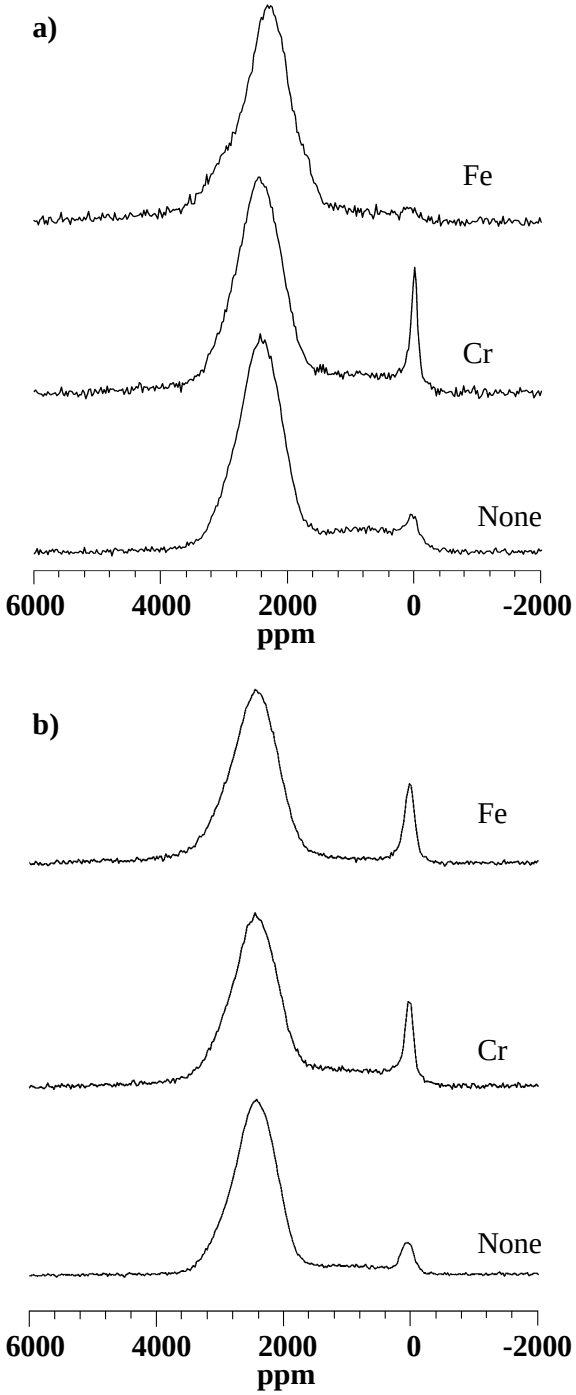

Figure 5-16. Wideline ^{31}P NMR spectra of promoted and unpromoted vanadyl pyrophosphate: a) freshly activated in butane/air, b) after 20 hours use in methane oxidation.

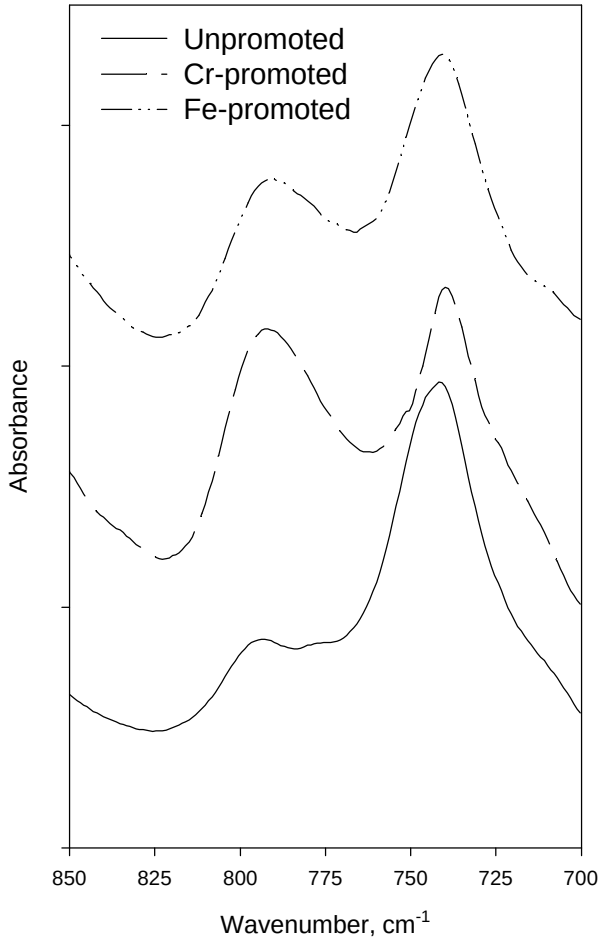

Figure 5-17. Infrared spectra (diffuse reflectance) showing the P-O-P symmetric stretch at 742 cm^{-1} and the V-(O=V) stretch at 795 cm^{-1}.

Mössbauer spectroscopy is a very powerful technique to probe the strength of bonding of a Mössbauer observable atom, which will give both qualitative and quantitative information on the oxidation state, covalency, coordination number and chemical environment. There is extensive literature on the application of this technique to characterize iron phosphates. A Mössbauer spectrum of the Fe-promoted VPO catalyst is shown in Figure 5-18. To our knowledge there is very little or no literature on the use of Mössbauer spectroscopy for Fe-promoted VPO catalysts even though Fe is a common component of industrial catalysts. The Fe content was only around 2% yet the Mössbauer spectrum was successfully acquired. The hyperfine interaction parameters as δ (Isomer shift relative to α-Fe in mm/s), Δ (Quadrupole splitting in mm/s) and Γ (Full-width-at-half-maximum in mm/s) are given in Table 5-5. Deconvolution of the peaks indicates presence of three susceptible components in this sample. Fractional resonance area (F) is for these components are tabulated in the last column of Table 5-5. The numbers in parenthesis indicates the variation in the last digit. The data indicate two forms of Fe^{3+} with the minor component being Fe^{2+}.

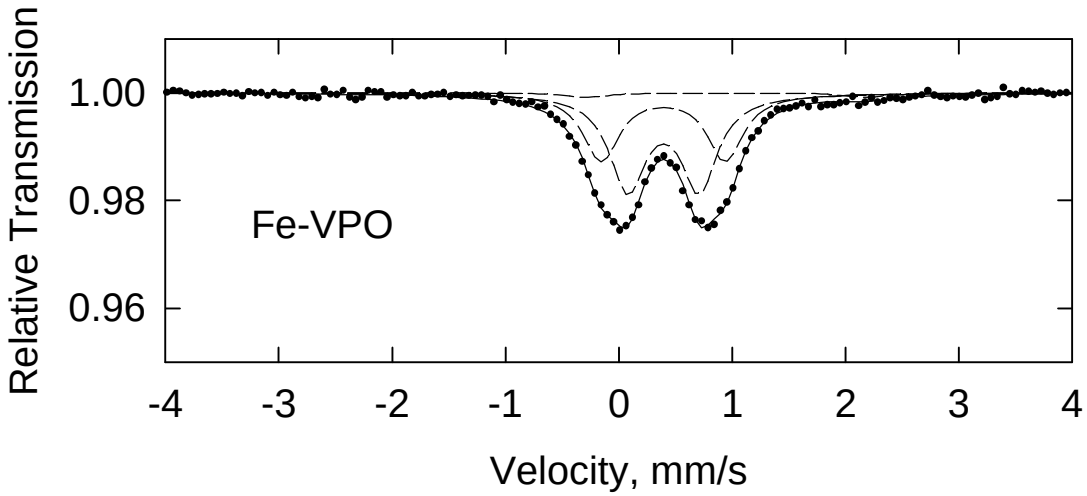

Figure 5-18. Mössbauer spectrum and fitted components for Fe promoted vanadyl pyrophosphate.

Table 5-5. Hyperfine Interaction Parameters for Fe-Promoted $(VO)_2P_2O_7$.

Catalyst	**Susceptible Component**	**δ (mm/s)**	**Δ (mm/s)**	**Γ (mm/s)**	**F (%)**
Fe-VPO	1	0.395 (5)	0.63 (1)	0.38 (2)	56
	2	0.393 (6)	1.10 (2)	0.38 (2)	40
	3	0.940 (6)	2.50 (2)	0.50 (1)	4

5.3.3. Methane Oxidation. The principal products of methane oxidation over VPO were found to be carbon monoxide and carbon dioxide, as noted in Section 5.1. Methane oxidation over the Cr and Fe promoted VPO catalysts was carried out at a fixed GHSV of 9300 h^{-1} and at a methane-to-oxygen ratio of 8.3. Selectivity as a function of methane conversion for these catalysts is shown in Figure 5-19. Formaldehyde was observed as a significant product in the reactor effluent for both Fe and Cr promoted VPO catalysts. Admittedly, conversions are very low in these experiments and not significant in an applied sense. However the point to be made is that in repeated experiments, no formaldehyde was observed over the unpromoted catalysts under nearly identical reaction conditions (lowest conversions in Figure 5-1) but formaldehyde was observed over the promoted samples. Large (up to 5 cm^3) GC sample loops were employed to amplify the formaldehyde signal in these runs. Formaldehyde peaks were five to six times greater than the noise level. Individual analyses as well as entire experiments were repeated with essentially the same results to with 10%.

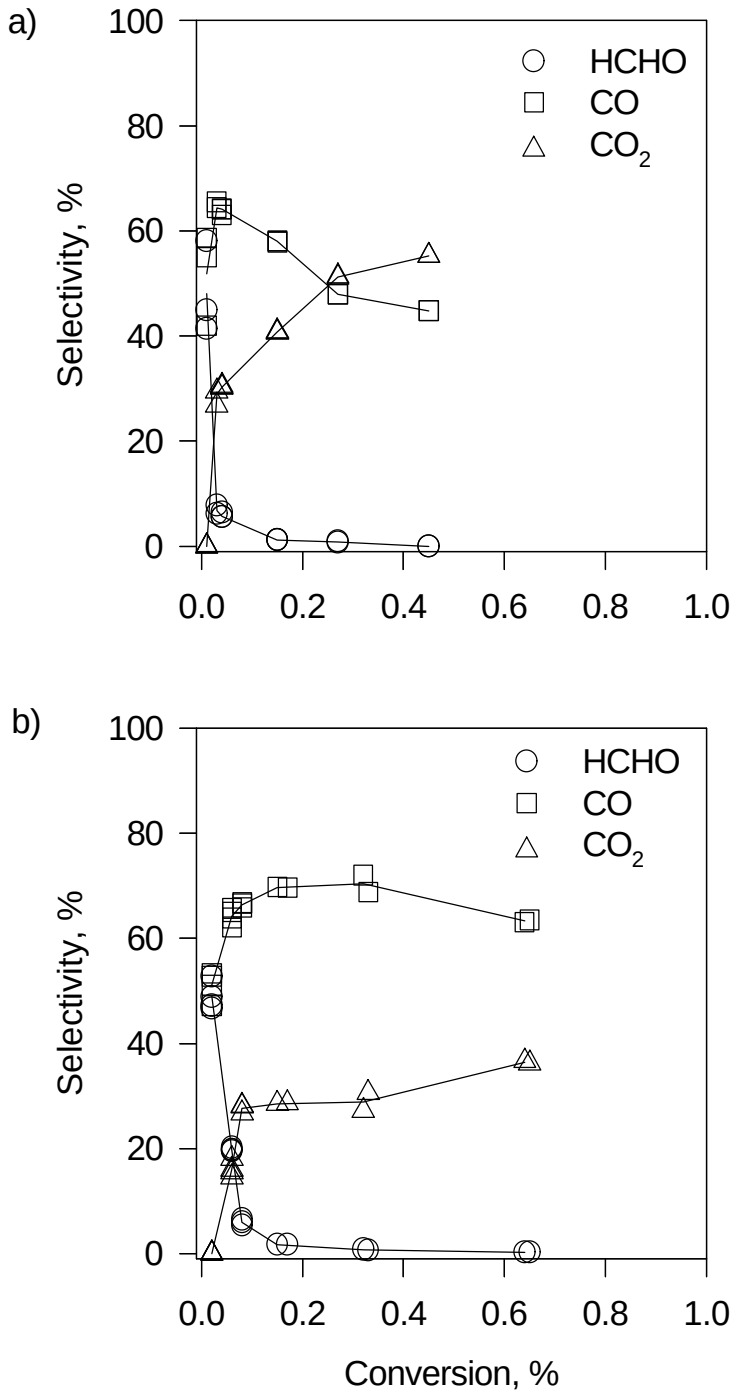

Figure 5-19. Product selectivity (%) as a function of methane conversion (%) for promoted vanadyl pyrophosphate catalysts. (a) Cr, (b) Fe.

In both promoted catalysts, at zero conversion formaldehyde selectivity approaches 100%, suggesting that it is the primary reaction product. Formaldehyde selectivity decreases rapidly as the extent of reaction increases. The increase in selectivity to carbon monoxide indicates that this compound is produced upon further oxidation of formaldehyde. Carbon dioxide became the

principal product at higher conversions. No CO_2 formation at low conversions indicates no direct oxidation route from methane to carbon dioxide. Assuming that the rate of methane oxidation has the same dependency on methane and oxygen partial pressures as the unpromoted catalyst, the Arrhenius relationships in Figure 5-20 were drawn and the Arrhenius parameters are listed in Table 5-6. Activation energies are essentially the same for the unpromoted, Fe, and Cr promoted catalysts.

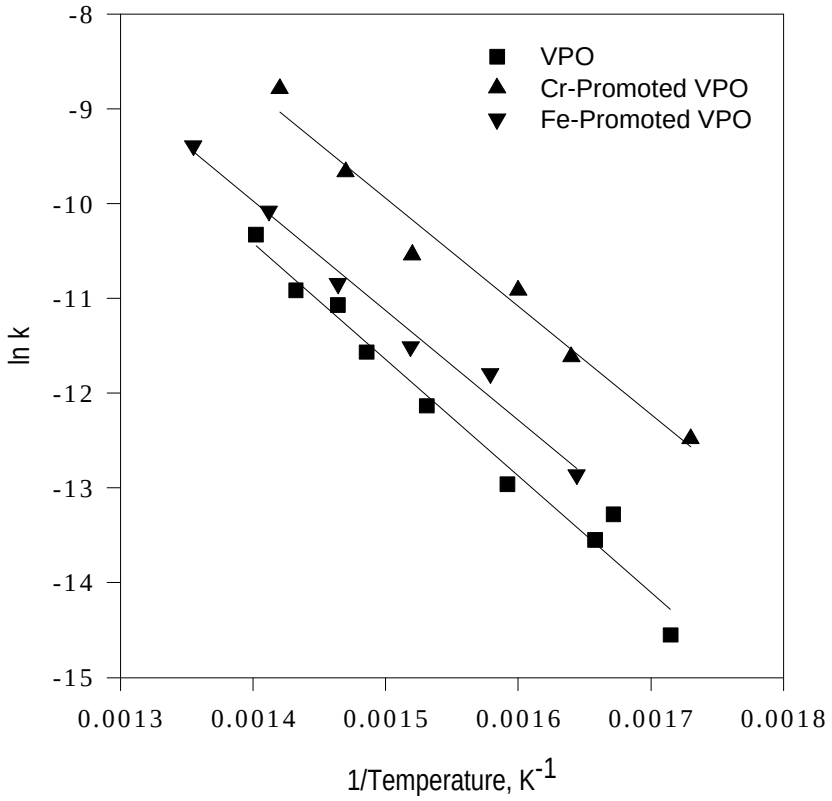

Figure 5-20. Arrhenius plot for methane oxidation reaction over promoted and unpromoted vanadyl pyrophosphate.

Table 5-6. Arrhenius parameters for methane oxidation over promoted and unpromoted VPO catalysts.

Catalyst	**Activation Energy, kJ/mole**	**Pre-exponential Factor, mole/g-min-atm$^{0.81}$**
VPO	102±6	860
Cr-VPO	95±8	1273
Fe-VPO	96±6	505

5.3.4. Discussion. The catalyst testing data indicate a sequential reaction path for methane oxidation over VPO and the promoted catalysts:

$$CH_4 + 1\ O_2 \xrightarrow{k_1} HCHO + H_2O$$

$$HCHO + 1/2\ O_2 \xrightarrow{k_2} CO + H_2O$$

$$CO + 1/2\ O_2 \xrightarrow{k_3} CO_2$$

Unpromoted vanadyl pyrophosphate is a poorly selective partial oxidation catalyst for the methane oxidation reaction. Carbon oxides and water are the principal products indicating that the ratio k_2/k_1 is large. A fractional order of 0.73 in methane partial pressure was observed. In the literature, with few exceptions, methane partial oxidation is assumed to be first order in methane and zero order in oxygen. Notably, Wang and Otsuka (1995) recently reported data that we have analyzed to yield a 0.68 order for methane oxidation over $FePO_4$ in the presence of hydrogen. A reaction order below unity indicates the existence of an inhibition (adsorption) term in a Langmuir-Hinshelwood type rate model. We interpret this to mean that as P_{CH4} increases, the surface becomes more reduced and sites capable of catalyzing oxidation become fewer. Reaction order for oxygen was found to be 0.08, very close to zero as expected for a redox or Mars and van Krevelen process with fast catalyst reoxidation. Promotion of VPO with Fe or Cr leads to the formation of measurable quantities of formaldehyde although space-time yields are low, typically between 0.5 and 2 g/kg-h. Low reaction temperatures and operation at very low methane conversion are required for formation of HCHO.

Characterization of promoted catalysts indicates that promoter elements are present on the surface and in the bulk at roughly 10:1 vanadium to promoter ratio. XRD indicates that vanadyl pyrophosphate is the main phase present, but promotion has resulted in several new peaks in the powder pattern, several of which can be assigned to α_{II}-$VOPO_4$. Examination of the (200) reflection at about 22.8 degree 2-theta suggests that promotion has not generated additional disorder (additional peak broadening) in the layer stacking and may have actually enhanced crystallinity in the Fe-promoted sample. Promotion appears to increase the average oxidation state (surface and bulk) of vanadium and, based on the IR spectral data, disrupts linkages between the layers of the structure.

We hypothesize that promoter atoms are incorporated between the layers and at the edges of the layers of these crystals rather than substituting for vanadium in the phosphate lattice. This is consistent with the method of promoter addition where promoters were added to the fully formed precursor. Perhaps the presence of these cations increases the degree of coordinative unsaturation of the surface vanadium centers favoring formation of oxidized vanadium as isolated V^V, or as V^V containing phase domains. Alternatively, promoters might activate oxygen more readily than VPO and catalyze oxidation of V^{IV} to form V^V. If promoter atoms are indeed at the edges of, or in between, the vanadyl pyrophosphate layers the promoter may enhance the ability of the structure to incorporate additional oxygen between the layers resulting in formation of V^V. A model where excess oxygen is incorporated between the layers has been discussed by Lopez Granados and coworkers (1993).

The presence of V^V is, of course, necessary for operation of a V^{IV}/V^V redox couple. Under butane oxidation conditions (1.5% butane in air) excess oxygen is present and the formation of V^V sites or phase domains is facile (Zhang-Lin, et al., 1994; Kiely, et al., 1996). Furthermore, using in-situ Raman studies of VPO activation in butane/air, Hutchings and coworkers (1994) observed the formation of V^V phases simultaneously with the start of maleic anhydride formation. Over the course of 20 hours the concentration of these phases increased, as did the selectivity to maleic anhydride. In a more recent in-situ x-ray absorption spectroscopy study, Coulston and coworkers (1997) concluded that V^V was involved in the reaction to form maleic anhydride and that V^{IV} was involved in reactions to form by-products. Production of maleic anhydride ended with removal of V^V from the catalyst by reduction and reaction of V^{IV} produced only carbon oxides. Thus there is considerable evidence that V^V species are necessary to form selective products under butane oxidation conditions.

Under methane oxidation conditions (in the range of 90% methane and 10% oxygen) there is no excess oxygen and formation of V^V may be unfavorable in unpromoted catalysts. The observation that the reaction order with respect to methane is less than unity may imply a loss of V^V sites capable of catalyzing oxidation as methane partial pressure is increased. Unfortunately, reaction order with respect to methane was not measured for the promoted catalysts. Promotion with Fe or Cr appears to stabilize or enhance the formation of V^V, as isolated sites or oxidized phase domains, and this may be responsible for the improved selectivity to partial oxidation products. Ben Abdelouahab and coworkers (1995) have reported a similar effect in butane oxidation for promotion by Fe and Co which were added as acetylacetonate salts during precursor preparation. Promotion enhanced the formation of a $VOPO_4$ structure at lower temperature and resulted in improved selectivity to maleic anhydride. While yields of selective oxidation products are quite low in the present study, the selectivity and characterization results support the notion that V^V is a necessary component of VPO surface sites capable of selectively oxidizing alkanes.

5.4. Oxidation of Methane by Unsupported Fe-Phosphates

Because of the positive results obtained for promotion of VPO with Fe, we have investigated methane oxidation over iron phosphates. At about the same time we were performing experiments with the Fe-promoted catalyst, Wang and Otsuka (1995) reported reasonable selectivity for formaldehyde in methane oxidation over $FePO_4$. Depending on the preparation and activation conditions and on the P:Fe ratio, $FePO_4$ can be prepared in two different structures. The first one is the well known quartz like phase structure with a P:Fe ratio of 1.0. This structure is comparable to that of SiO_2 due to the alternated substitution of one FeO_4 tetrahedron and one PO_4 tetrahedron for two SiO_4 tetrahedra. A tridymite type phase is also observed in the presence of an excess of phosphorous, and it can be stabilized at lower temperatures (733-803 K). The $FePO_4$ material was the first iron phosphate selected for study.

5.4.1. Catalyst Preparation. $FePO_4$ was prepared using the method described by Wang and Otsuka (1995). A stoichiometric, aqueous solution of $Fe(NO_3)_3$ and $NH_4H_2PO_4$ was prepared and dried at 363 K for 12 hr. The precipitate obtained was calcined at 823 K for 5 hr in air. Wang and Otsuka report the surface area of this material to be 8.5 m^2/g. For samples prepared with P:Fe=1 calcination at 773 K produces the tridymite form and calcination above 823 K

produces the quartz form (Muneyama, et al, 1996). These is some evidence that employing a P:Fe ratio of 1.3 can stabilize the tridymite form at higher temperatures as can the addition of Cs (Millet and Vedrine, 1991).

$Fe_4(P_2O_7)_3$ was prepared from $Fe_4O_{21}P_6 \cdot xH_2O$ (~20% water), which can be prepared by heating ferric nitrate and diammonium hydrogen phosphate up to 1123 K (Bonnet, et al., 1996). The precursor was activated in an air stream for 24 h, at 773 K. Activation above this temperature caused significant visual structural transformations. XRD patterns indicated an amorphous structure both for the precursor and activated catalyst.

5.4.2. Catalyst Characterization. Results of BET surface area measurements for these iron phosphates are listed in Table 5-7. Surface area of the $FePO_4$ catalyst reported in the literature ranges form 1.8 to 15 m^2/g (Bonnet, et al., 1996 and Ai, et al., 1993), which is consistent with our results.

Table 5-7. BET Surface Area Measurement for Iron Phosphate Catalysts.

Catalysts	Surface Area (m^2/g)
$FePO_4$(Q)	8.6±0.2
$Fe_4(P_2O_7)_3$	9.1±0.2

X-ray diffraction patterns for unsupported $FePO_4$(Q), both fresh and after roughly 30 hours of use in methane oxidation, are reported in Figure 5-21. The most intense peaks at 25.6 and 20.1 degree two theta are characteristic of the quartz form of this material. No major changes occurred during use in methane oxidation although the used catalyst may be slightly more crystalline given the greater sharpness and intensity of its main peaks. There appears to be a slight offset between the patterns of the fresh and used catalysts but this is believed to be an experimental artifact rather than an actual change in lattice parameter.

Mossbauer spectra for $FePO_4$ (Q) and for a sample with a high P:Fe ratio and stabilized with Cs to contain $FePO_4$ (T) are reported in Figure 5-22. Two forms of Fe^{3+} are evident in both spectra, however significant differences exist in the coordination and relative amounts of these two forms. Hyperfine interaction parameters are reported in Table 5-8 which confirm this observation. While Mossbauer is a particularly powerful technique for characterizing iron phosphates, data interpretation is non-trivial and a detailed interpretation did not evolve during this project.

Table 5-8. Hyperfine Interaction Parameters for Fe-P-O Catalysts.

Catalyst	**Susceptible Component**	**δ (mm/s)**	**Δ (mm/s)**	**Γ (mm/s)**	**F (%)**
$FePO_4$ (T) w/ Cs (P:Fe=2.33)	1	0.447 (3)	0.39 (1)	0.35 (1)	68
	2	0.424 (5)	0.85 (2)	0.40 (1)	32
$FePO_4$ (Q)	1	0.282 (5)	0.62 (1)	0.29 (1)	93
	2	0.300 (1)	0.90 (1)	0.30 (1)	7

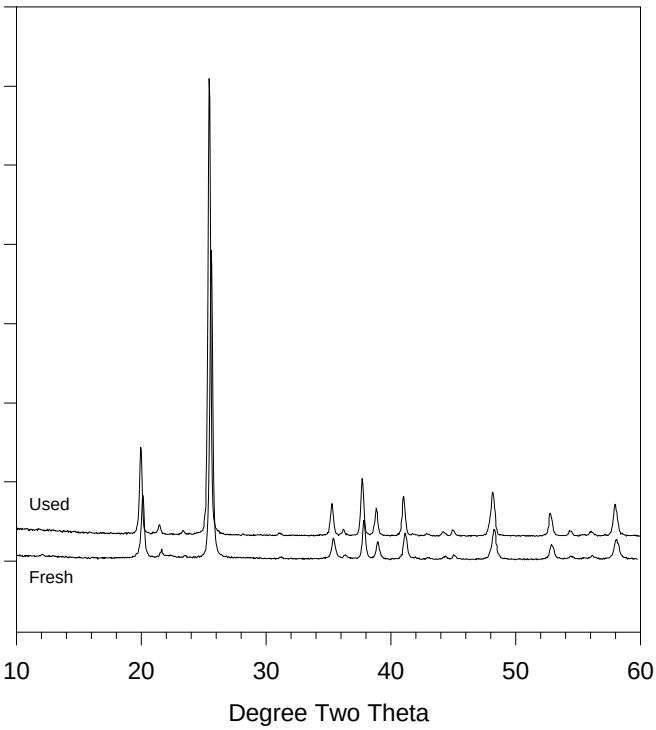

Figure 5-21. X-ray diffraction data for $FePO_4$(Q) before and after use in methane oxidation.

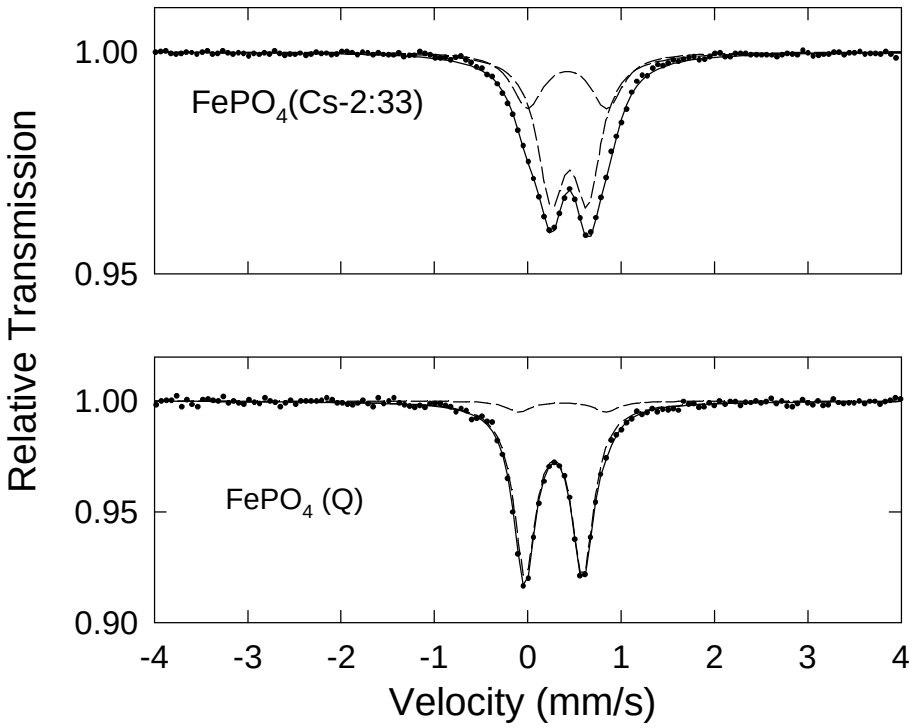

Figure 5-22. Mossbauer spectra of a) the tridymite phase of $FePO_4$, with an P:Fe ratio of 2.33. 8% wt. Cs was used in the preparation to promote the formation of the tridymite phase, and b) the quartz phase of $FePO_4$ with P:Fe ratio of 1.

5.4.3. Methane Oxidation. The quartz phase of $FePO_4$ was investigated in detail for CH_4 oxidation. Formaldehyde was the only selective product observed in these experiments. The conversion-selectivity plot presented in Figure 5-23 indicates that HCHO selectivity is higher at lower CH_4 conversion levels. CO selectivity approaches zero at very low conversions which suggests that it is a secondary product. Interestingly, even at low conversion conditions, CO_2 selectivity is high. This may be explained with the presence of a direct oxidation path from CH_4 to CO_2.

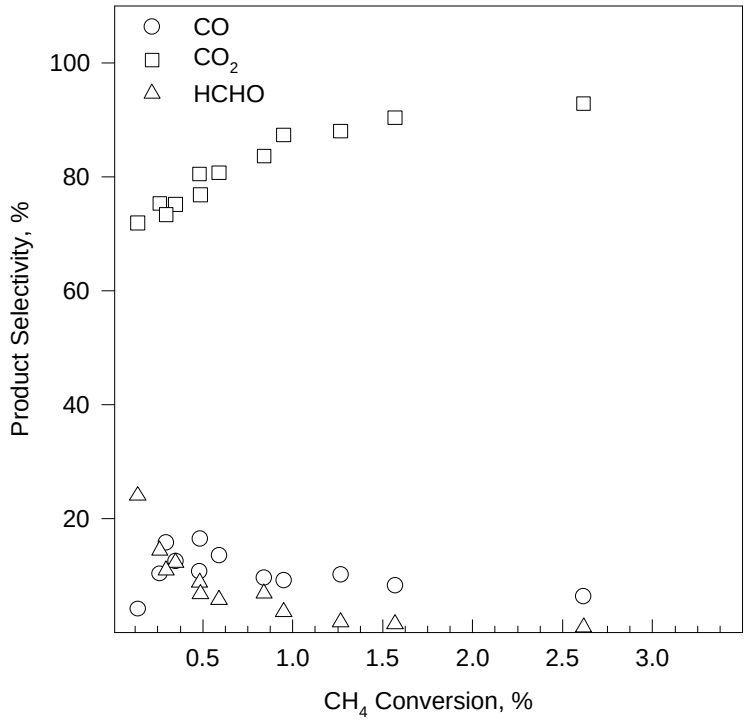

Figure 5-23. Product selectivity as a function of CH_4 conversion over $FePO_4$(Q) catalyst. P_{CH4} = 37.6 kPa, P_{O2} = 3.1 kPa, CH_4:O_2 = 12 ,GHSV = 10,000 - 30,000 hr^{-1}, T= 848-898 K.

The effect of temperature on methane conversion rate was examined and an Arrhenius plot for these data, assuming first order in methane and zero order in oxygen, is shown in Figure 5-24. For CH_4/O_2=2.15, E_a=91.6±7.5 and for CH_4/O_2=8.32, E_a=69.9±15.5 kJ/gmol. It seems likely that the activation energy is unaffected by CH_4/O_2 and the best estimate of E_a is the average value of 80.8 kJ/gmol. Effect of CH_4 and O_2 partial pressures were examined in order to determine optimum operating conditions to maximize formaldehyde yields. The slope of the lines in Figures 5-25 and 5-26 represents the reaction orders of CH_4 and O_2 for a power law rate model. Reaction orders for CH_4 and O_2 were calculated as 0.66 and 0.45, respectively. These experiments were repeated at different temperatures, and the influence of temperature on the reaction orders was found to be negligible in the range studied. This is a relatively high reaction rate dependence on oxygen for a partial oxidation catalyst. For example the VPO catalyst exhibited an order of only 0.1 in oxygen and most studies assume zero order. If we assume the

Mars and van Krevelen model, this implies that hydrocarbon oxidation and surface reoxidation occur at comparable rates.

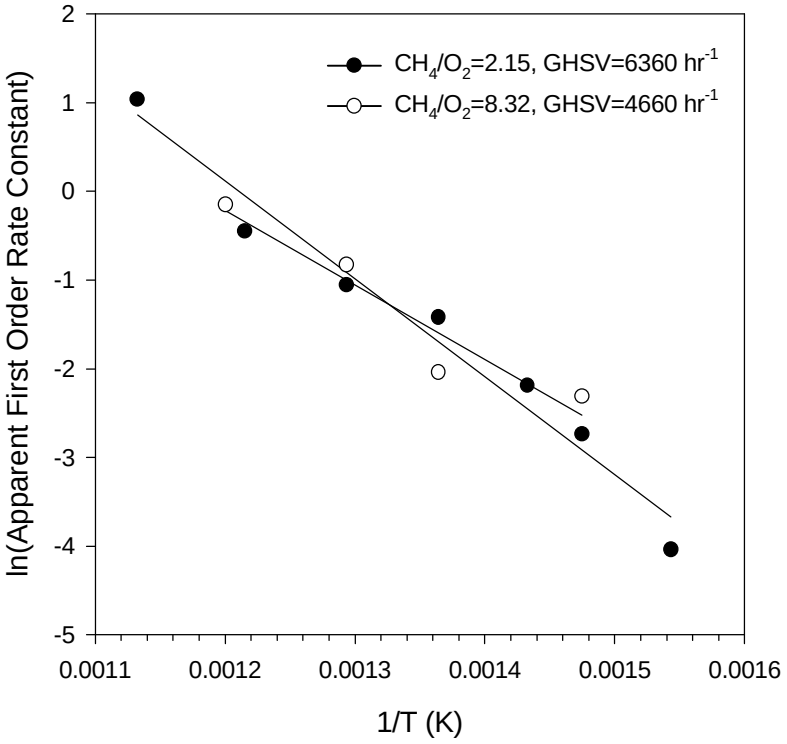

Figure 5-24. Arrhenius plot for methane oxidation over $FePO_4$.

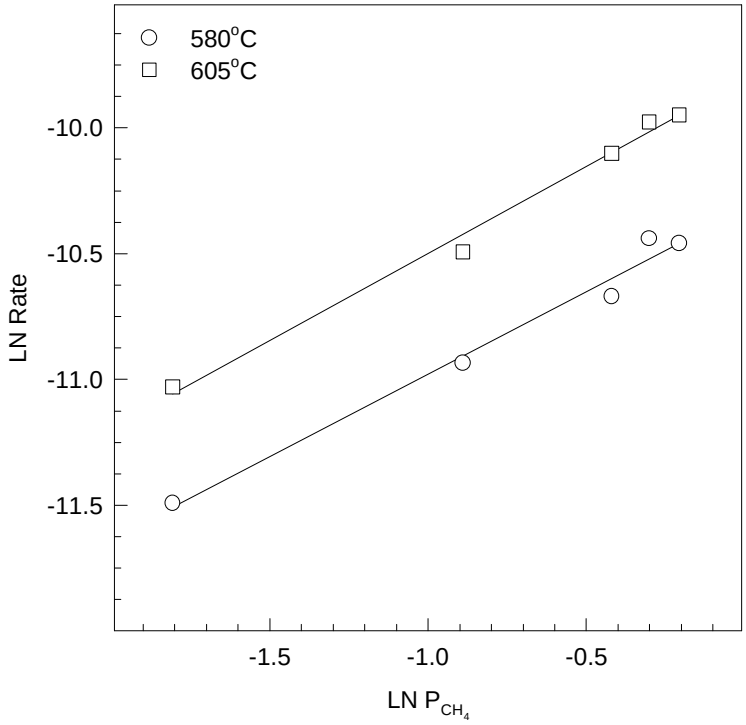

Figure 5-25. Effect of CH_4 partial pressure on CH_4 oxidation rate over $FePO_4$(Q) catalyst. P_{CH4} = 16.7-82.2 kPa, P_{O2} = 3.1 kPa, GHSV = 12,750 hr^{-1}.

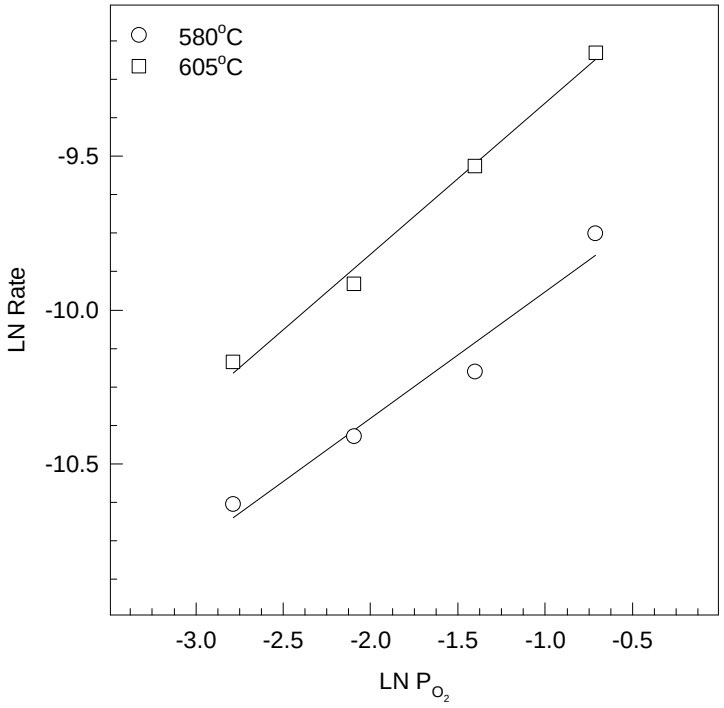

Figure 5-26. Effect of O_2 partial pressure on CH_4 oxidation rate over $FePO_4$(Q) catalyst. P_{CH4} = 49.8 kPa, P_{O2} =6.2-49.8 kPa, GHSV = 12,750 hr^{-1}.

It is well known that in the presence of steam the iron phosphates can form mixed valence hydroxyphosphates that are active and selective catalysts for other oxidation reactions (Millet and Vedrine, 1995), so the use of steam was attempted. As the selectivity-conversion plot presented by Figure 5-27 indicates, the presence of steam in the feed stream causes a decrease in the CO_2 selectivity and appears to eliminate the direct pathway from methane to CO_2. CO and HCHO selectivity increases when steam is co-fed. During these experiments, steam partial pressure was varied in 3.1 to 9.3 kPa range, keeping the GHSV constant.

The effect of CH_4, O_2 and H_2O partial pressures on space time yield of formaldehyde are presented by Figure 5-28. Feeding steam with the reacting mixture has significant effects on formaldehyde yield and selectivity. Highest formaldehyde space time yield observed for the $FePO_4$(Q) in the absence and in the presence of steam were 59 and 148 g/kg h, respectively. In these experiments no methanol was observed. High O_2 partial pressure as well as CH_4 partial pressure promoted the formaldehyde yield.

Thus, $FePO_4$ exhibits dramatically higher yields of formaldehyde than the Fe-promoted VPO catalysts described before. However a space time yield of 148 g/kg-h is still roughly one order of magnitude too low for commercial application.

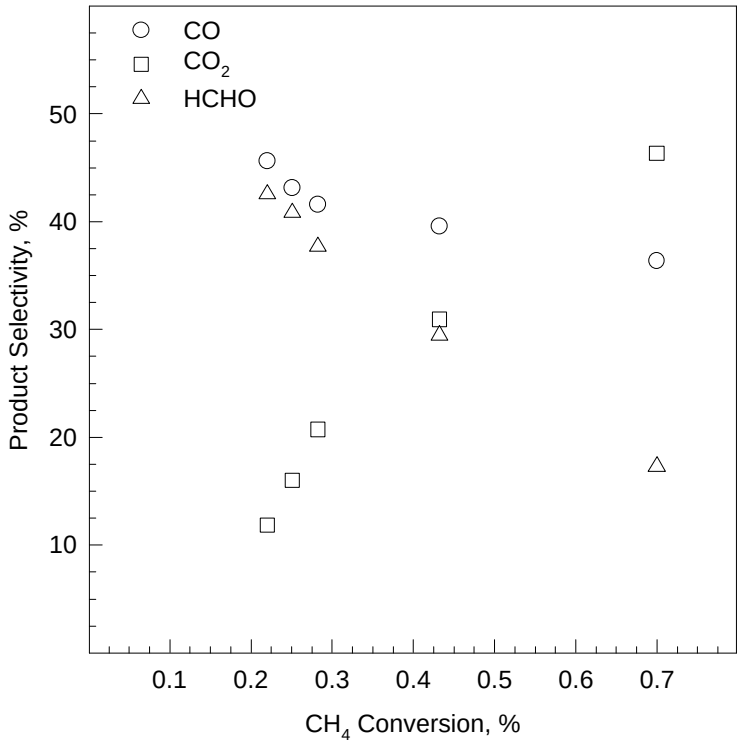

Figure 5-27. Product selectivity as a function of CH_4 conversion over $FePO_4$(Q) in the presence of water in the feed stream. P_{CH4} = 37.6 kPa, P_{O2} = 3.1 kPa, P_{H2O} = 3.1 kPa, CH_4:O_2 = 12 , GHSV = 10,000 - 30,000 hr^{-1}, T= 848-898 K.

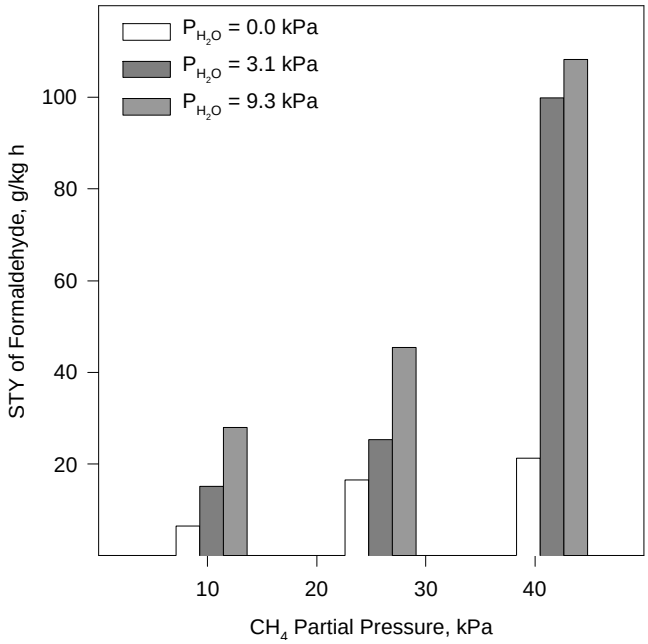

a)

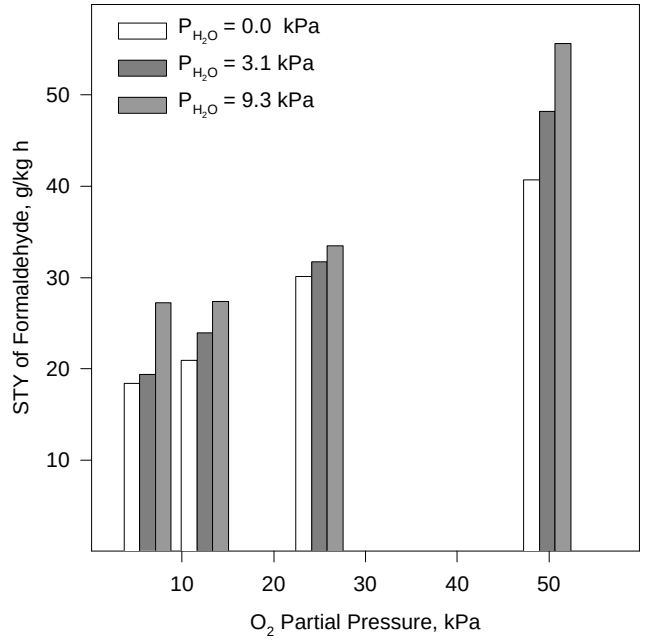

b)

Figure 5-28. Effect of (a) CH_4 partial pressure with P_{O2}=6.2 kPa and (b) O_2 partial pressure with P_{CH4}=49.9 kPa, on STY of HCHO in the absence and presence of water.

5.5. Oxidation of Methane by $FePO_4$ Supported on SiO_2

Many of the most active and selective methane partial oxidation catalysts known are supported on silica, and silica itself is an active and selective catalyst for formaldehyde

formation. We discovered that preparation of $FePO_4$ on silica was easily accomplished and then investigated this catalyst for methane partial oxidation.

5.5.1. Catalyst Preparation. Silica supported $FePO_4$ was prepared from a precipitated, acid washed silica by incipient wetness impregnation with a solution of $Fe(NO_3)_3$ and $NH_4H_2PO_4$ with a target iron loading of 5wt%. This material was dried and calcined at 900 K/18 hr. The activity for methane conversion of the silica support was also investigated. Two different silica supports prepared by precipitation SiO_2-OR (99.6%, BDH Chemicals) and SiO_2-AW (99.8%, Cerac Chemicals) were investigated in detail. In the literature, it was speculated that even traces of Na may cause significant deactivation of the catalyst. These silica supports were washed with a nonpolar acid to reduce the Na content. The not-acid-washed silicon oxide catalyst, SiO_2-NAW (99.8% Cerac Chemicals), was also tested.

5.5.2. Catalyst Characterization. Results of BET surface area measurements of the several SiO_2 and the supported catalyst sample are listed in Table 5-9.

Table 5-9. BET Surface Area Measurement for Supported Fe-P-O and SiO_2 Catalysts.

Catalysts	**Surface Area (m^2/g)**
$FePO_4(Q)/SiO_2$ (5%)	80.8±1.8
SiO_2-OR	140.4±3.1
SiO_2-NAW	621±13
SiO_2-AW	588±13

Different precipitated silicon oxides yielded significant differences in the surface area. We can speculate that the SiO_2-AW contains micropores that lead to a four-fold increase in the surface area. A 40 m^2/g decrease in the surface area indicates that acid washing promotes the collapse of some of these pores. Silica supported $FePO_4(Q)$ catalyst has a significantly lower surface area than the support itself (SiO_2-OR). Such a decrease in the surface area can be explained by pore blocking caused by $FePO_4(Q)$ clusters. The loading level for this catalyst was 5% wt. Lower loading levels of $FePO_4(Q)$ may prevent excessive pore blocking and result in a more active catalyst.

Figure 5-29 reports x-ray diffraction data for the silica supported $FePO_4$ as well as the amorphous silica support. The main peak of $FePO_4(Q)$ is evident in the fresh catalyst and this peak as well as the second most intense peak are much more intense in the used sample. Apparently an activation or sintering process is occurring. In addition to the XRD results, X-ray photoelectron spectroscopy has been performed on the fresh silica supported sample. The data indicate an atomic P:Fe ratio of approximately 4, compared to the bulk ratio of 1. Thus the surface of this material is substantially enriched in phosphorus. We speculate that this surface enrichment isolates the Fe-O active sites by surrounding them with phosphate groups and leads to the selective catalytic behavior we have observed.

A Mossbauer spectrum for this catalyst is shown in Figure 5-30. Two Fe^{3+} components are observed. The hyperfine interaction parameters as δ (Isomer shift relative to α-Fe in mm/s), Δ (Quadrupole splitting in mm/s) and Γ (Full-width-at-half-maximum in mm/s) are given in Table 5-10. Deconvolution of the peaks confirms the presence two susceptible components. Fractional

resonance area (F) is for these components is tabulated in the last column of Table 5-10. The numbers in parenthesis indicates the variation in the last digit. A more detailed interpretation of these data was not possible within the scope of this project.

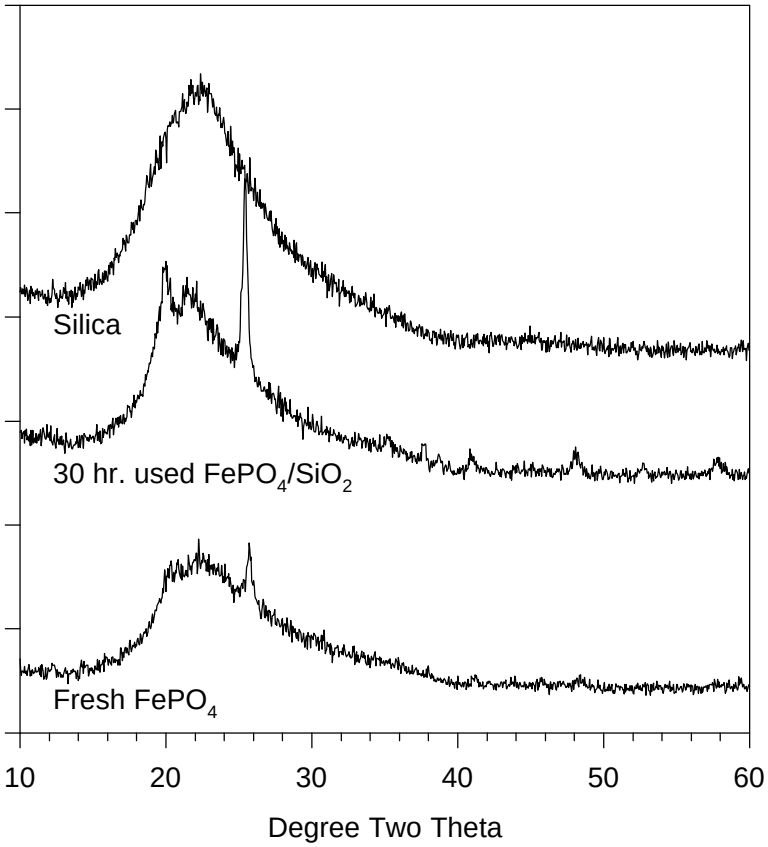

Figure 5-29. X-ray diffraction data for $FePO_4$(Q) supported on silica, as well as the silica support, before and after use in methane oxidation.

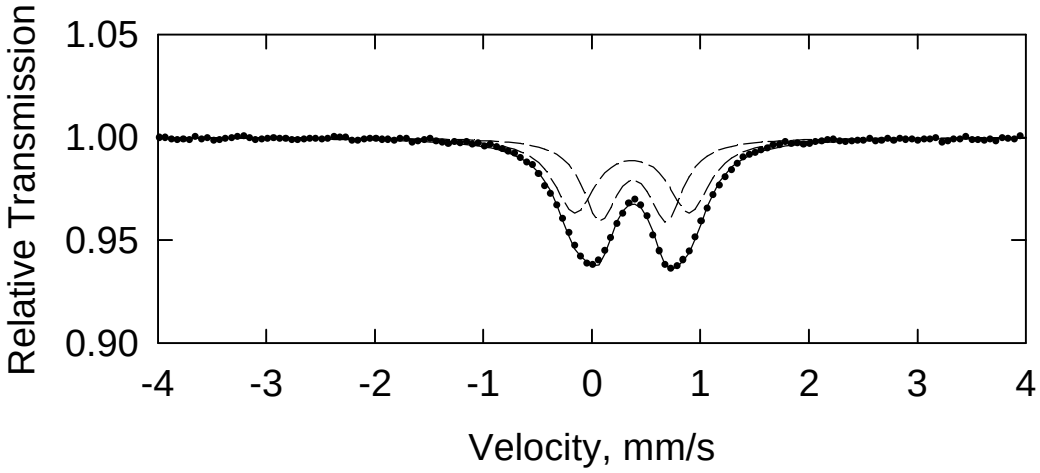

Figure 5-30. Mossbauer spectrum of 5% $FePO_4$ supported on silica.

Table 5-10. Hyperfine Interaction Parameters for Supported Fe-P-O Catalysts.

Catalyst	Susceptible Component	δ (mm/s)	Δ (mm/s)	Γ (mm/s)	F (%)
$FePO_4(Q)/SiO_2$	1	0.380 (4)	0.61 (2)	0.38 (1)	47
	2	0.372 (4)	0.06 (3)	0.46 (1)	53

5.5.3. Methane Oxidation over Silica Support. The activity of the support was measured to determine the best material for this application. Silicon oxide catalysts prepared by different methods were tested and significantly different catalytic activity and selectivity patterns were observed for these different preparations (also discussed in the literature by Parmaliana, et al., 1991). Among these preparations, fumed silica (99.8%, Aldrich) was found to be the least active, while the silica prepared by precipitation was the most active one.

Product selectivity as a function of methane conversion over the SiO_2-AW catalyst is presented by Figure 5-31. In these experiments, conversion was varied by varying the space time. Experiments were repeated in the temperature range of 848 to 898 K. HCHO selectivity was observed to be high at low methane conversion levels and decreases to 20% at 1% conversion. CO_2 was the principal product above 1% conversion. CO selectivity increases as formaldehyde selectivity goes down, which indicates sequential oxidation of formaldehyde to CO. High CO_2 selectivity even at very low conversion levels suggests a direct oxidation route from CH_4 to CO_2,which is also observed for V_2O_5/SiO_2 systems (Spencer, et al., 1989). Formaldehyde space time yields (STY) in the range of 7-113 g/kg h were observed over the SiO_2-AW. Interestingly, higher formaldehyde yields were observed at high oxygen partial pressures. Formaldehyde selectivity, on the other hand, was favored at low oxygen concentrations (i.e. high CH_4:O_2 ratio).

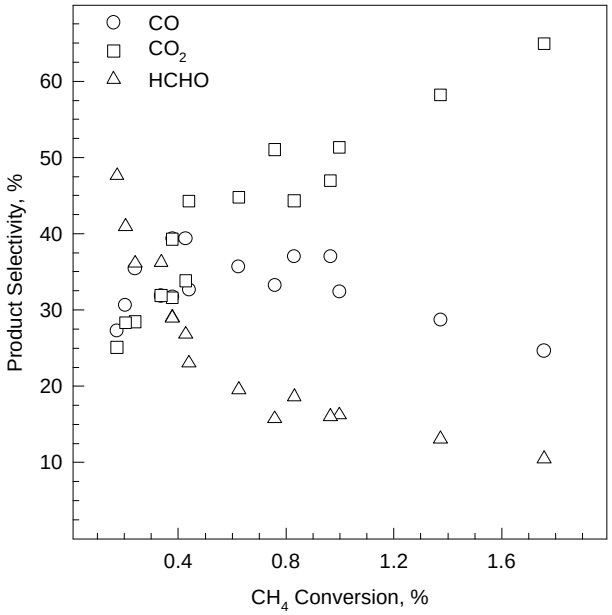

Figure 5-31. Product selectivity as a function of CH_4 conversion over SiO_2-AW catalyst. P_{CH4} = 37.6 kPa, P_{O2} = 3.1 kPa, CH_4:O_2 = 12 ,GHSV = 10,000 - 30,000 hr^{-1}, T= 848-898 K.

Selectivity-conversion pattern observed for the SiO_2-OR presented in Figure 5-32 was found to be very similar to that of SiO_2-AW catalyst. Even though the surface area of the SiO_2-OR catalyst is much lower, it is a more active catalyst than SiO_2-AW for CH_4 oxidation. Formaldehyde selectivity, at 1% conversion, was about 10% over SiO_2-OR, which is slightly lower than the one observed for SiO_2-AW. For the SiO_2-OR catalyst space time yield of formaldehyde was slightly lower than the SiO_2-AW (in the range of 5 to 92 g/kg h). For the supported iron phosphate catalyst preparations SiO_2-AW was be used as the support material.

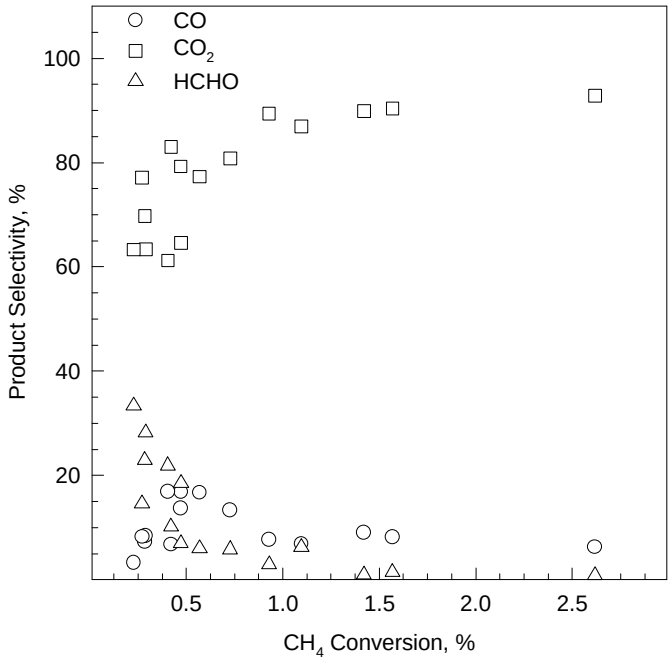

Figure 5-32. Product selectivity as a function of CH_4 conversion over SiO_2-OR catalyst. P_{CH4} = 37.6 kPa, P_{O2} = 3.1 kPa, CH_4:O_2 = 12 , GHSV = 10,000 - 30,000 hr^{-1}, T= 848-898 K.

To determine the reaction orders in oxygen and methane (α and β), partial pressures of these species were kept constant one at a time while varying the other, and the reaction rate was measured. Gas hourly space velocity (GHSV) was also kept constant in these experiments. Effect of methane and oxygen partial pressures on the reaction rate is given in Figure 5-33 and 5-34. A power law rate model was applied to describe the kinetics of methane oxidation over SiO_2-AW and SiO_2-OR catalysts.

$$-r_{CH4} = k\, P_{CH4}^{\alpha}\, P_{O2}^{\beta}$$

The reaction orders for methane and oxygen were calculated as 0.91 and 0.32, and 0.93 and 0.31 for SiO_2-AW and SiO_2-OR catalysts, respectively, essentially identical values. A first order reaction in CH_4 partial pressure agrees with the reported literature (Parmaliana, et al., 1991), but a fractional reaction order of 0.3 in O_2 partial pressure is quite unusual for CH_4 oxidation catalysts. Previously, over the vanadium phosphate systems we have reported very little or no dependence on the oxygen concentration, but oxygen concentration effects the methane oxidation rate positively in the case of silicon oxide catalysts.

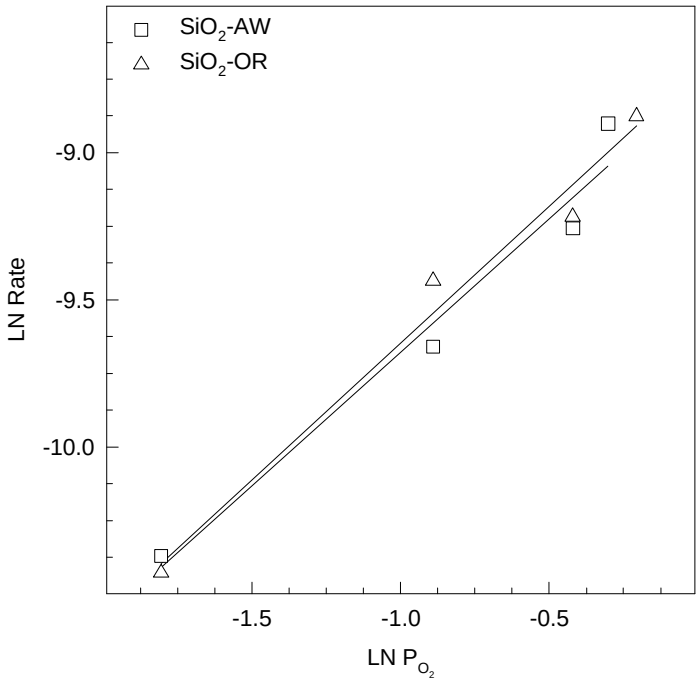

Figure 5-33. Effect of CH_4 partial pressure on CH_4 oxidation rate over SiO_2-AW and SiO_2-OR catalysts. P_{CH4} = 16.7-82.2 kPa, P_{O2} = 3.1 kPa,GHSV = 12,750 hr^{-1}, T=873 K.

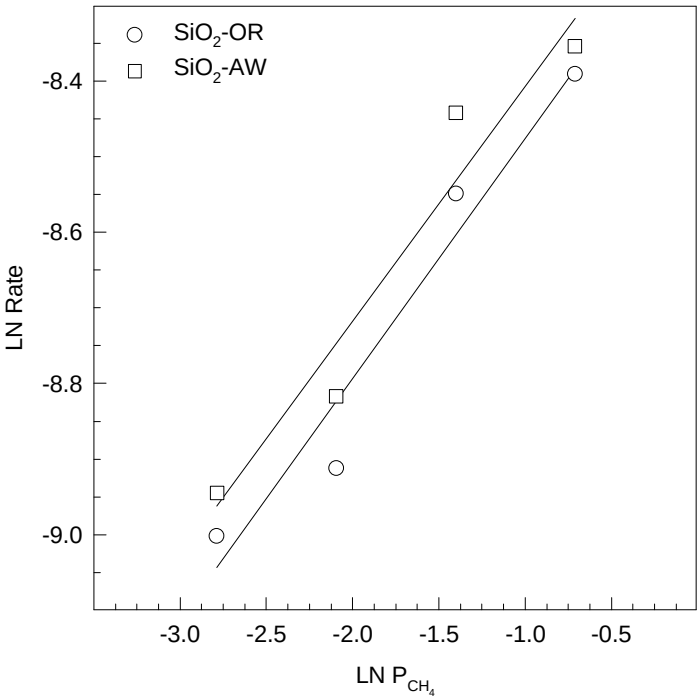

Figure 5-34. Effect of O_2 partial pressure on CH_4 oxidation rate over SiO_2-AW and SiO_2-OR catalysts. P_{CH4}= 49.8 kPa, P_{O2} =6.2-49.8 kPa, GHSV = 12,750 hr^{-1}, T = 873 K.

Activation energy of methane oxidation over the SiO_2-AW and SiO_2-OR was also calculated as 184 and 142 kJ/mole, respectively. An Arrhenius plot is given in Figure 5-35 for these catalysts. This activation energy value is very typical to the ones reported in the literature for different silica preparations (Kastanas, et al., 1988). The linear nature of this plot even at the highest conversion levels insures the absence of mass and heat transfer effects. Pore diffusion limitation is particularly important to avoid, since the SiO_2-AW is an extremely high surface area catalyst (~600 m^2/g).

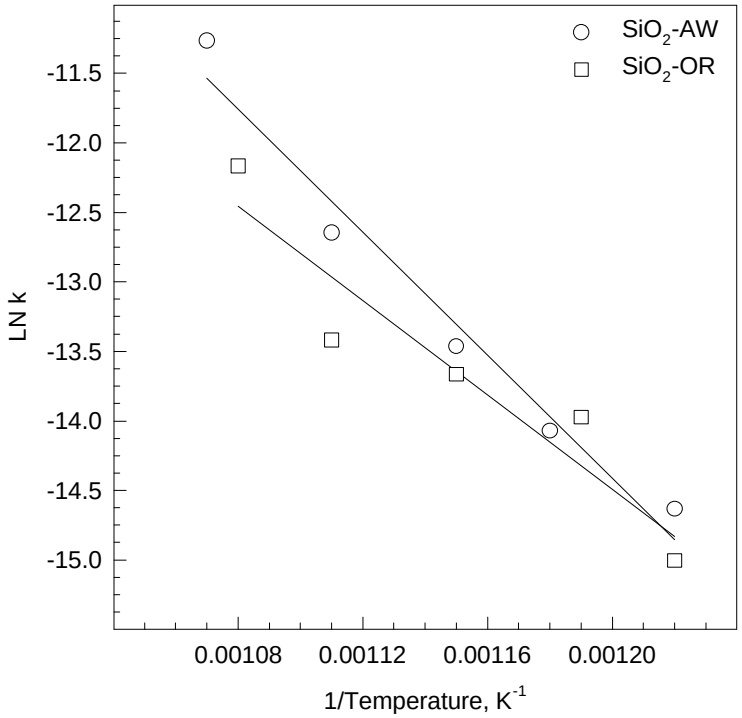

Figure 5-35. Arrhenius plot for CH_4 oxidation over SiO_2-AW and SiO_2-OR catalysts. P_{CH4} = 50.1 kPa, P_{O2} = 3.1 kPa, CH_4:O_2 = 12, GHSV = 21,000 hr^{-1}, T= 823-933 K.

The effect of acid washing on the catalytic activity was also tested for SiO_2 catalysts. The not-acid-washed silicon oxide, SiO_2-NAW catalyst, was found to be less active than nitric acid washed SiO_2-AW. Formaldehyde selectivity and space time yield were also lower for the SiO_2-NAW. Figure 5-36 presents a comparison of the methane conversion and formaldehyde space time yield for the acid washed and not-acid-washed precipitated silicon oxide catalysts.

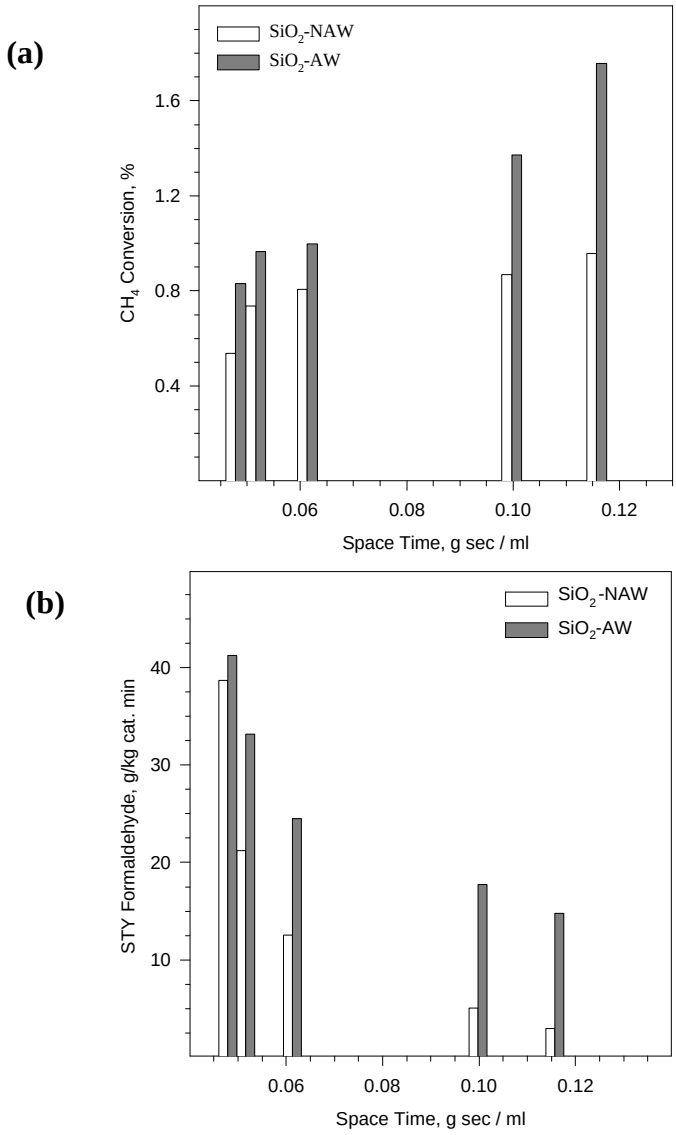

Figure 5-36. Comparison of (a) CH_4 conversion, (b) Formaldehyde STY for regular and acid washed SiO_2 catalysts. P_{CH4}= 16.7-82.2 kPa, P_{O2}= 3.1 kPa, GHSV= 12,750 hr^{-1}, T=873 K.

5.5.4. Methane Oxidation over $FePO_4/SiO_2$. Supporting $FePO_4$(Q) with silicon oxide caused an appreciable synergetic effect on the catalytic activity and selectivity. Quantifiable amounts of methanol and high formaldehyde space time yields were observed. A selectivity-conversion plot for this catalyst is presented in Figure 5-37 . These results indicate that 40% formaldehyde selectivity can be achieved over 1-2% conversion level. These data indicate the following reaction path:

$$CH_4 \longrightarrow HCHO \longrightarrow CO \longrightarrow CO_2$$

Space time yields of HCHO and CH_3OH as a function of CH_4:O_2 ratio are given in Figure 5-38. Methane formation into methanol was more favorable if the CH_4:O_2 ratio was kept high (i.e. 22.5 and above). On the other hand, higher space time yield of formaldehyde can be achieved at

higher oxygen partial pressure levels. Higher STY of formaldehyde was observed at higher temperatures, but CH_3OH formation is favorable at relatively low temperatures (i.e. 858 K).

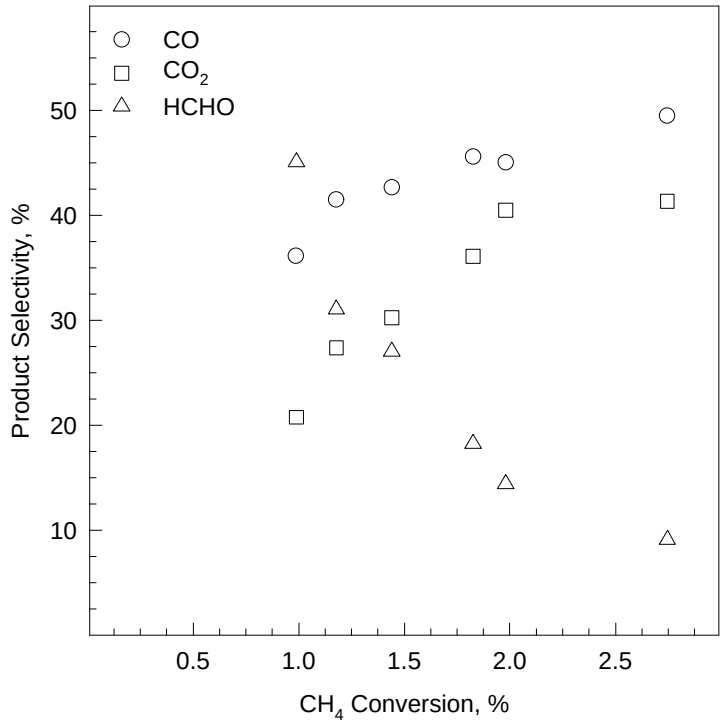

Figure 5-37. Product selectivity as a function of CH_4 conversion over $FePO_4(Q)/SiO_2$ catalyst. P_{CH4} = 37.6 kPa, P_{O2} = 3.1 kPa, CH_4:O_2 = 12 , GHSV = 10,000 - 30,000 hr^{-1}, T= 898 K.

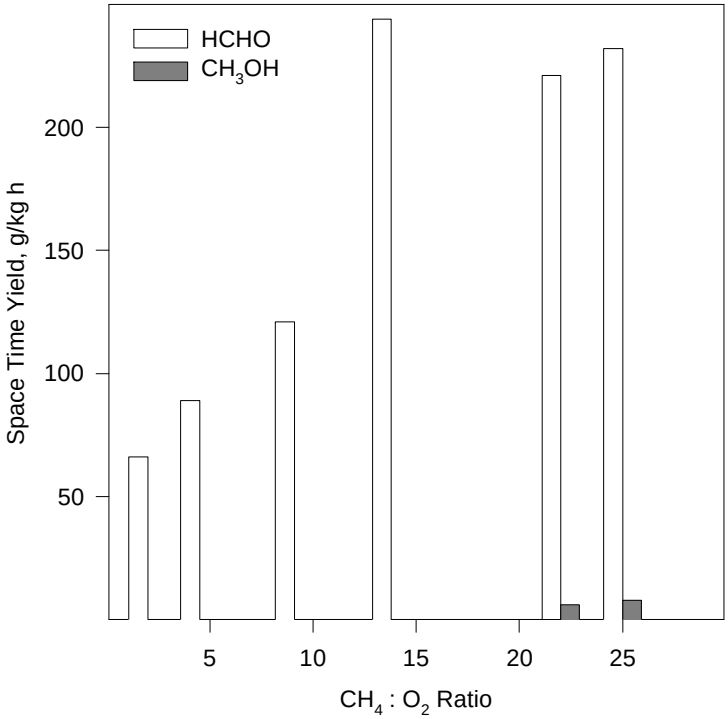

Figure 5-38. Space time yields of HCHO and CH_3OH over the $FePO_4(Q)/SiO_2$ as a function of CH_4:O_2 ratio. GHSV = 12,750 hr^{-1}, T= 858 K.

Conversion as a function of temperature for two CH_4/O_2 ratios is reported in Figure 5-39. As for the unsupported catalyst, CH_4/O_2 ratio has no effect on methane oxidation rate. An Arrhenius plot of these data, assuming first order in methane and zero order in oxygen, is reported in Figure 5-39. The activation energies of 141.4±10.5 at CH_4/O_2=1.54 and 116.7±19.7 kJ/gmol at CH_4/O_2=8.32 are not different and the average value is 129.3 kJ/gmol. This value is significantly higher than the 80.8 kJ/gmol observed for the unsupported catalyst and is similar to the value of 136.0 kJ/gmol that we have observed for methane oxidation over just the silica support. The meaning of this increase in activation energy upon supporting $FePO_4$ on silica is unclear at this time.

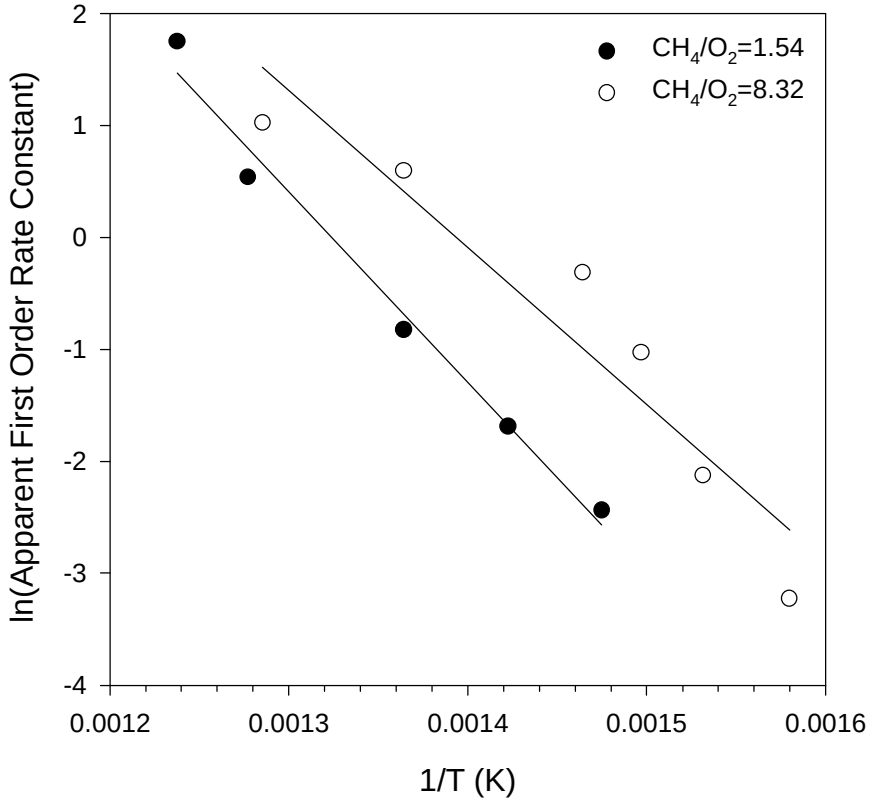

Figure 5-39. Arrhenius plot for methane oxidation over silica supported $FePO_4$, 5wt% loading.

To determine the effect of methane partial pressure on methane oxidation rate methane partial pressure was changed in the range of 16.7 to 82.2 kPa, keeping the oxygen partial pressure constant at 3.1 kPa. A simple power law model was applied to describe the kinetics of methane oxidation. The reaction orders in CH_4 and O_2 were determined as described earlier in this report. Methane oxidation rate as a function of methane partial pressure is presented in Figure 5-40. Reaction order for CH_4 was calculated to be 0.61.

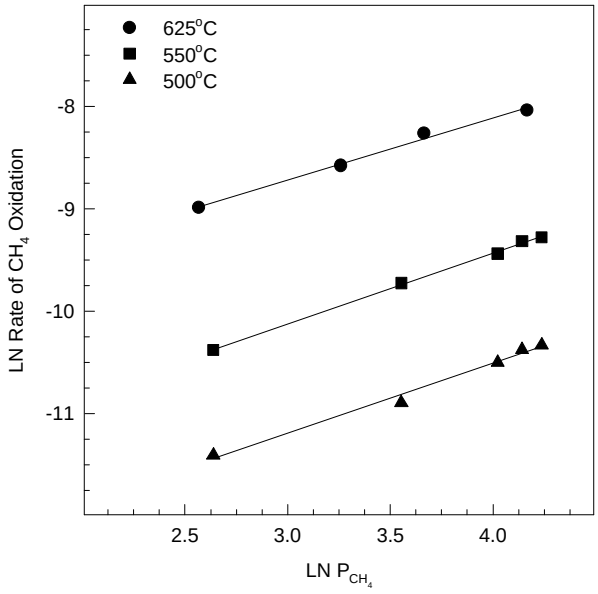

Figure 5-40. Effect of CH_4 partial pressure on CH_4 oxidation rate over $FePO_4(Q)/SiO_2$ catalyst. P_{CH4} = 16.7-82.2 kPa, P_{O2} = 3.1 kPa, GHSV = 12,750 hr^{-1}.

To determine the reaction order of oxygen for a power law rate model, oxygen partial pressure was changed in the range of 6.2 to 50.0 kPa, while keeping the methane partial pressure constant at 3.5 kPa. Results of these experiments are presented in Figure 5-41. Reaction order for oxygen was found to be 0.28. Experiments were repeated in the temperature range of 550-650°C range, to observe the dependence of reaction order on temperature and no such dependence have been observed, in the temperature range studied.

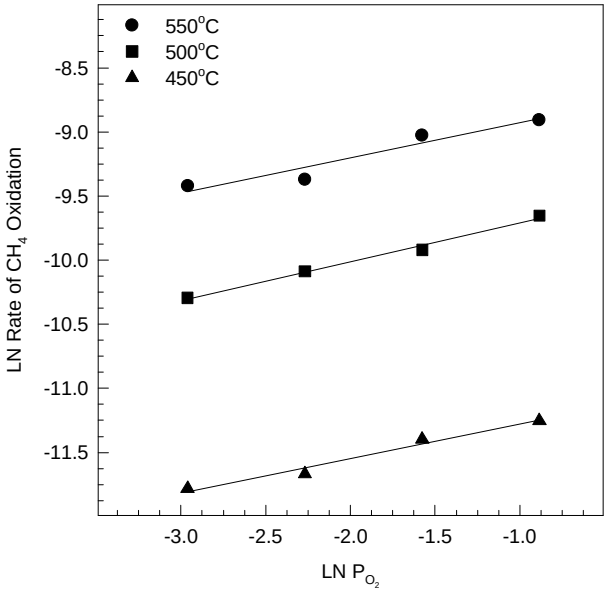

Figure 5-41. Effect of O_2 partial pressure on CH_4 oxidation rate over $FePO_4(Q)/SiO_2$ catalyst. P_{CH4} = 49.8 kPa, P_{O2} =6.2-49.8 kPa, GHSV = 12,750 hr^{-1}.

Effect of steam in the feed stream was also investigated. Steam partial pressure in the feed was varied in the range of 3.1 to 9.0 kPa. The effect of steam on selectivity with 3.9 kPa of water is shown in Figure 5-42. As was observed for unsupported $FePO_4$, steam leads to a substantial improvement in formaldehyde selectivity. Data obtained at two methane/oxygen ratios and two temperatures are reported in Figure 5-42. The data for CO and HCHO fall on the same curve for both sets of conditions, however the data for CO_2 selectivity are significantly lower at the lower methane/oxygen ratio. The effect of methane/oxygen ratio on HCHO space time yield is reported in Figure 5-43. The highest space time yield of HCHO obtained was nearly 500 g/kg-h and was produced with 3.1 kPa of water and a methane to oxygen ratio of 0.75. The fact that high yields can be obtained over this catalyst at high oxygen partial pressures is very unusual in methane oxidation. Typically yields of selective products are insignificant for methane to oxygen ratios below about 5. Here we observe little sensitivity to methane to oxygen ratio above a value of about 2.

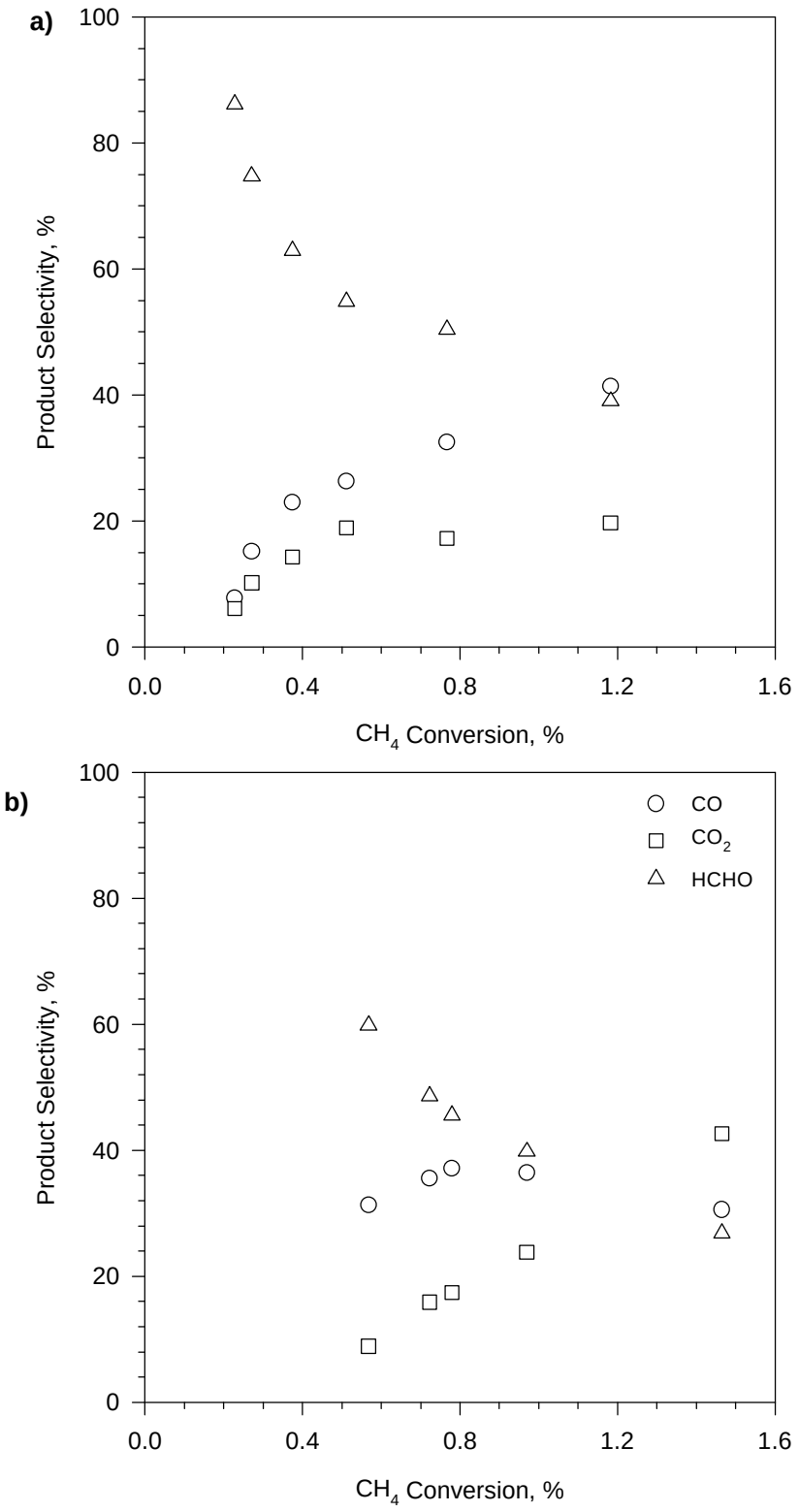

Figure 5-42. Product selectivity as a function of CH_4 conversion over $FePO_4(Q)/SiO_2$ catalyst in the presence of steam. P_{CH4} = 28 kPa, P_{O2} = 14 kPa, P_{H2O} = 3.9 kPa CH_4:O_2 = 2 , GHSV = 2,500 - 21,000 hr^{-1}, T= 823 K, b) P_{CH4} = 32 kPa, P_{O2} = 2.7 kPa,P_{H2O} = 3.9 kPa CH_4:O_2 = 12 , GHSV = 9,700 - 20,300 hr^{-1}, T= 873 K.

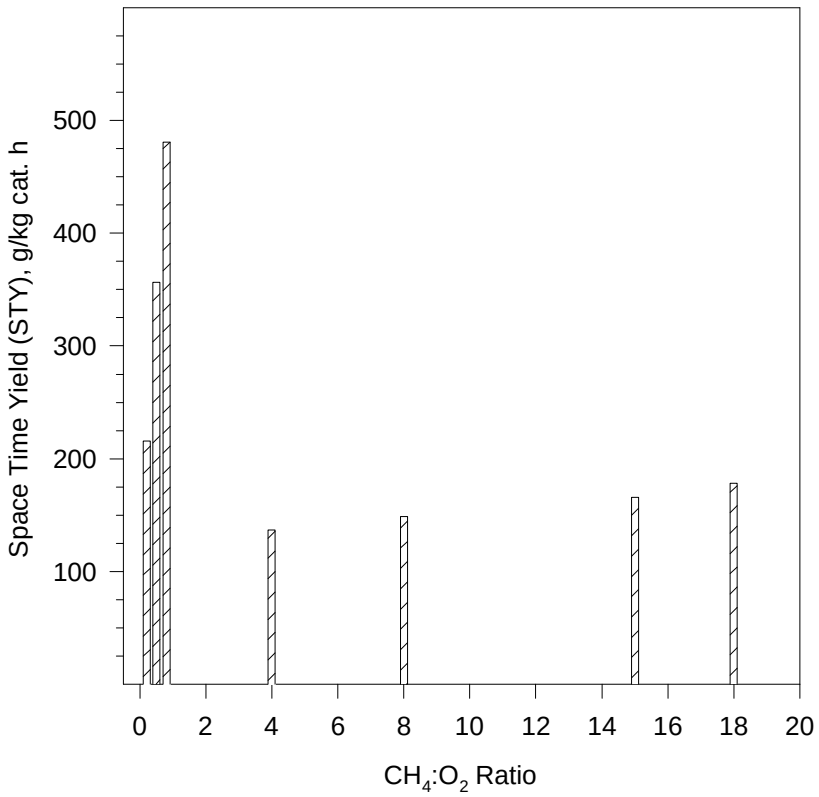

Figure 5-43. Effect of methane to oxygen ratio on space time yield of formaldehyde for $FePO_4$ supported on silica in the presence of steam.

The effect of steam on reaction orders was also investigated and the results of these experiments are reported in Figure 5-44. The reaction orders were found to be 0.48 for methane, 0.21 for oxygen, and 0.23 for water. The plot is not particularly linear for water suggesting a more complex behavior than can be modeled by a simple power law approach. This very surprising result of a positive reaction order in water deserves some discussion. Because water is a reaction product for most of the reactions occurring in this system, it was anticipated that adding water to the feed would inhibit the rate of methane conversion. That fact that water enhances the rate implies that water is causing formation of a new active site, perhaps through formation of one of the iron hydroxyphosphate phases.

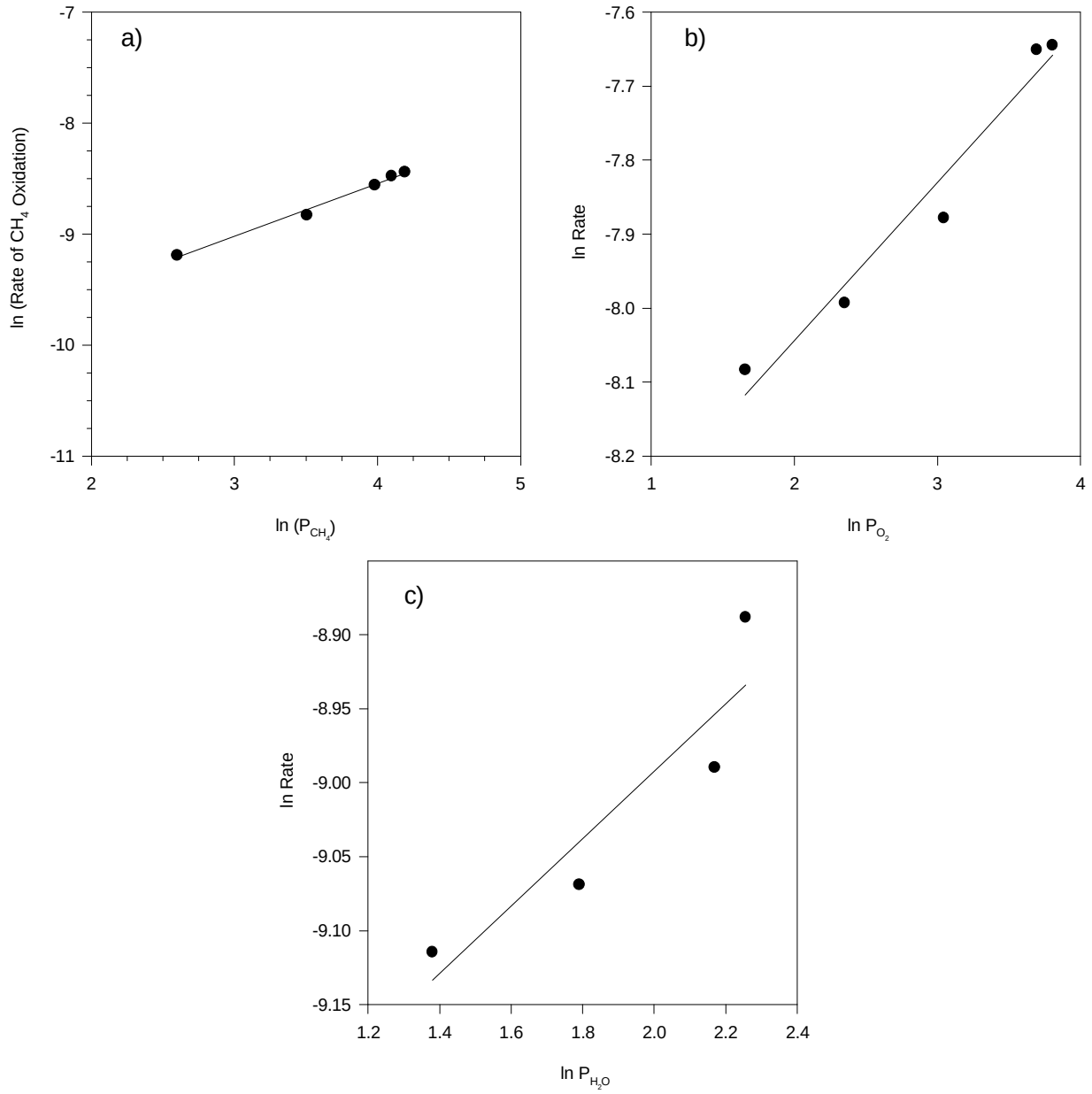

Figure 5-44. Reaction order determination over $FePO_4$ supported on silica: a) For methane, P_{CH4} = 13.5-66 kPa, P_{O2} = 2.9 kPa, P_{H2O} = 3.9 kPa, GHSV = 10,000 hr^{-1}, T= 873 K, b) For oxygen, P_{CH4} = 41 kPa, P_{O2} = 5.2-45 kPa,P_{H2O} = 3.9 kPa, GHSV = 10,000 hr^{-1}, T= 873 K, c) For water, P_{CH4} = 32 kPa, P_{O2} = 2.7 kPa,P_{H2O} = 3.9-9.6 kPa, GHSV = 10,000 hr^{-1}, T= 873 K.

In summary, supported iron phosphate catalysts produce high yields of formaldehyde and measurable yields of methanol from methane under some reaction conditions. The fact that high oxygen partial pressures can be employed may have important implications for process economics in direct methane partial oxidation. These catalytic materials have not been widely studied but have a rich solid state and surface chemistry. An understanding of what unique properties of these materials lead to high selectivity in methane partial oxidation may prove

beneficial. Furthermore, it is also possible that a thorough study of methane oxidation over iron phosphate and related materials will lead to the discovery of highly active and selective catalysts.

6. SUMMARY AND CONCLUSIONS

This DOE sponsored study of methane partial oxidation began with testing of vanadyl pyrophosphate (VPO), a well-known alkane selective oxidation catalyst. It was found that VPO was not a selective catalyst for methane conversion yielding primarily CO. However, promotion of VPO with Fe, Cr, and other first row transition metals led to measurable yields for formaldehyde, as noted in Table 6-1. Yields with vanadium phosphate catalysts were extremely low and it was decided to pursue another strategy. Given that Fe successfully promoted VPO, and given Wang and Otsuka's (1995) report that $FePO_4$ had interesting properties for methane oxidation, it this phosphate was selected for additional study. $FePO_4$ (quartz polymorph) was found to be a much more active and selective catalyst than VPO producing formaldehyde at nearly two orders of magnitude higher yield (see Table 6-1). When this material was supported on silica, yield again nearly doubled. Inclusion of steam in the feed gas lead to a further doubling of yield. Measurable but low yields of methanol were also observed.

Table 6-1. Kinetic Parameters and Yields for CH_4 Oxidation over Various Catalysts.

Catalyst	**Reaction Order**			**Activation Energy, kJ/mol**	**Maximum Space Time Yield, g/kg-h**	
	CH_4	**O_2**	**H_2O**		**HCHO**	**CH_3OH**
$(VO)_2P_2O_7$	0.73	0.08	--	102	0	0
$(VO)_2P_2O_7$-Fe	--	--	--	96	1.5	0
$(VO)_2P_2O_7$-Cr			--	95	2.0	0
$FePO_4$ (Q)	0.66	0.45	--	81	59	0
					148[a]	
SiO_2 OR	0.93	0.31	--	142	96	0
$FePO_4/SiO_2$	0.61	0.28	--	129	240	5
	0.48	0.21	0.23	--	487	8

[a]In the presence of steam.

The iron phosphate system consists of a number of Fe^{2+}, Fe^{3+}, and mixed valence phosphates and hydroxyphosphates (Ai, et al., 1993; Bonnet et al., 1996; Millet and Vedrine, 1991; Muneyama, et al., 1996). The fact that water enhances selective product yields and exhibits a positive effect on the methane conversion rate strongly suggests the formation of a hydroxyphosphate under our reaction conditions. An extremely interesting feature of the silica supported iron phosphate catalyst is that high formaldehyde yields could be obtained at very low methane to oxygen ratios (even below 1). This behavior is extremely unusual in methane partial oxidation and may have significant practical and economic implications, notably elimination of the need to use pure oxygen. Future studies should focus on the effect of water and oxygen partial pressure on surface structure, and how changes in structure lead to formation of methanol.

Aspects of the work described in this final report were presented at the 1997 North American Catalysis Society Meeting in Chicago, and will appear shortly in a refereed journal. A second

journal article is currently undergoing peer review and a third is in preparation. Results for the iron phosphate materials will be presented at the 1997 AIChE Meeting in Las Angeles.

7. REFERENCES

Ai, M. J. Catal. 101 389 (1986).

Ai, M., Muneyama, E., Kunishige, A., Ohdan, K., J. Catal. 144 632 (1993).

Ben Abdelouahab, F., Olier, R., Guilhaume, N., Lefebvre, F., and Volta, J.C. J. Catal. 134, 151 (1992).

Ben Abdelouahab, F., Olier, R., Ziyad, M., and Volta, J.C. J. Catal. 157, 687 (1995).

Bonnet, P., Millet, J.M.M., J. Catal. 161 198 (1996).

Busca, G., et al., J. Catal. 99 400 (1986a).

Busca, G., et al., J. Phys. Chem. 90 1337 (1986b).

Busca, G. and Centi, G. J. Am. Chem. Soc. 111 46 (1989).

Cavani, F. and Trifiro, F. Chemtech April, pp. 18 (1994).

Centi, G., et al., Chem. Rev. 88 55 (1988).

Cornaglia, L.M., et al., Appl. Catal. 74 15 (1991).

Cornaglia, L.M., et al., Appl. Catal. 95 117 (1993a).

Cornaglia, L.M., et al., Appl. Catal. 100 37 (1993b).

Cornaglia, L.M., and Lombardo, E.A. Appl. Catal. A General 127, 125 (1995).

Coulston, G.W., Thompson, E.A., and Herron, N., J. Catal. 163, 122 (1996).

Coulston, G.W., Bare, S.R., Kung, H., Birkeland, K., Bethke, G.K., Harlow, R., Herron, N., and Lee, P.L. Science 275, 191 (1997).

Ebner, J.R. and Thompson, M.R. Catal. Today 16 51 (1993).

Garbassi, F., Bart, J., Tassinari, R., Vlaic, G., and Laborde, P., J. Catal. 98, 317 (1986).

Gay, I., J. Phys. Chem. 75 10 (1971).

Hodnett, B.K. Catal. Rev. Sci. Eng. 27 373 (1985).

Holstein, W.L. and Machiels, C.W. J. Catal. 162 118 (1996).

Horowitz, H.S., et al., Appl. Catal. 38 193 (1988).

Hutchings, G.J. Appl. Catal. 72 1 (1991).

Hutchings, G.J., Desmartin-Chomel, A., Olier, R., and Volta, J.-C. Nature 368, 41 (1994).

Hutchings, G.J., and Higgins, R. J. Catal. 162, 153 (1996).

Johnson, J.W., et al., J. Am. Chem. Soc. 106 8123 (1984).

Kastanas, G.N., Tsigdinos, G.A., Schwank, J., J. ACS Div. Petr. Chem. Prepr. 33 3 393 (1988).

Kiely, C.J., Burrows, A., Sajip, S., Hutchings, G.J., Sananes, M.T., Tuel, A., and Volta, J.C. J. Catal. 162, 31 (1996).

Li, J., Lashier, M.E., Schrader, G.L., and Gerstein, B.C. Appl. Catal. 73, 83 (1991).

Lopez Granados, M., Conesa, J.C., and Fernandez-Garcia, M. J. Catal. 141, 671 (1993).

Lopez Granados, M., and Wolf, E.E., Applied Cat. A:General, 131**,** 263 (1995).

Michalakos, P.M., et al., J. Catal. 140 226 (1993).

Millet, J.-M. M., Vedrine, J.C. Appl. Catal. 76 209 (1991).

Moser, T.P., and Schrader, G.L. J. Catal. 104, 99 (1987).

Muneyama, E., Kunishige, A., Ohdan, K., Ai, M. J. Catal. 158 378 (1996).

Otake, M. U.S. Patent 4,337,173, January 29, 1982.

Parmaliana, A., Frusteri, F., Miceli, D., Mezzapica, A., Scurell, M.S., Giordiano, N., Appl. Catal. 78 7 (1991).

Parmialiana, A., et al., J. Catal. 148 514 (1994).

Pepera, M.A., et al., J. Am. Chem. Soc. 107 4883 (1985).

Sananes-Schulz, M.T., Ben Abdelouahab, F., Hutchings, G.J., and Volta, J.C. J. Catal. 163, 346 (1996).

Spencer, N.D., Pereira, C.J. J. Catal. 116 399 (1989).

Takita, Y., Tanaka, K., Ichimaru, S., Mizihara, Y., Abe, Y., and Ishihara, T. Appl. Catal. A: General 103, 281 (1993).

Wang, Y., and Otsuka, K., J. Catal. 155**,** 256 (1995).

Watson, I.M., Connor, J.A., and Whyman, R. Thin Solid Films 201, 337 (1991).

Zhang-Lin, Y., Forissier, M. Vedrine, J.C., and Volta, J.C. J. Catal. 145, 267 (1994).